VARIATIONAL ANODIC OXIDATION OF ALUMINUM FOR THE FORMATION OF CONICALLY PROFILED NANOPOROUS ALUMINA TEMPLATES

By

Patrick D. Wallace

RECOMMENDED:

Advisory Committee Chair

Chair, Department of Physics

APPROVED:

Dean, College of Natural Science and Mathematics

Dean of the Graduate School

April 9, 2012

Date

VARIATIONAL ANODIC OXIDATION OF ALUMINUM FOR THE FORMATION OF CONICALLY PROFILED NANOPOROUS ALUMINA TEMPLATES

A

THESIS

Presented to the Faculty

of the University of Alaska Fairbanks

in Partial Fulfillment of the Requirements

for the Degree of

MASTERS OF SCIENCE

By

Patrick D. Wallace, B.S.

Fairbanks, Alaska

May 2012

Abstract

Anodic oxidation of metals, otherwise known as anodization, is a process by which the metal in question is intentionally oxidized via an electrochemical reaction. The sample to be oxidized is connected to the anode, or positive side of a DC power source, while a sample of similar characteristics is attached to the cathode or negative side of the same power source. Both leads are then immersed in an acidic solution called the electrolyte and a current is passed between them. Certain metals such as aluminum or titanium anodized in this way form a porous oxide barrier, the characteristics of which are dependent on the anodization parameters including the type of acid employed as the electrolyte, pH of the electrolyte, applied voltage, temperature and current density. Under specific conditions the oxide formed can exhibit highly ordered cylindrical nanopores uniformly distributed in a hexagonal pattern. In this way anodization is employed as method for nanofabrication of ordered structures.

The goal of this work is to investigate the effects of a varied potential difference on the anodization process. Specifically to affect a self-assembled conical pore profile by changing the applied voltage in time. Although conical pore profiles have been realized via post-processing techniques such as directed wet etching and multi-step anodization, these processes result in pore dimensions generally increasing by an order of magnitude or more. To date there has been reporting on galvanostatic or current variations which directly effected the resulting pore profiles, but to our knowledge there has not been a reported investigation of potentiostatic or voltage variation on the anodization process.

We strive to realize a conical pore profile in process with the traditional two-step anodization method while maintaining the smallest pore dimensions possible. Pores having diameters below 20nm with aspect ratios about 1.0 would be ideal as those dimensions would be much closer to some of the characteristic lengths governing the quantum confined spatial domain. Thus we set out to answer the question of what effect a time varied potential difference will have on the traditional two-step anodization method, a technique we refer to as *variational anodization*, and if in fact conically profiled nanopores can be realized via such a technique.

Table of Contents

List of Figures

Page

Page

List of Tables

Page

Acknowledgements

We would like to acknowledge the University of Alaska Graduate School for their generous fellowship which afforded bread and warmth through the early years of this work.

Also the Physics Department for their contribution of high purity aluminum and other materials with out which this work could not have been.

And finally the Center for High Technology Materials at the University of New Mexico for providing the analysis needed to conclude this work.

Chapter 1
Introduction

For many years now nanotechnology has represented a major front in scientific and engineering advancements. The potential for innovation within this field of solid sate and quantum physics was first recognized by Richard Feynman, who during his 1959 address to the American Physical Society stated "In the year 2000, when they look back at this, they will wonder why it was not until the year 1960 that anybody began to seriously move in the direction."[1] This direction of course began the scaling down of ordinary matter to finite collections of tens to hundreds of atoms.

For the majority of known elements such a collection would have dimension on the order of hundreds of angstroms to tens of nanometers. The tremendous capacity for innovation associated with such a material regime is attributable to the alteration of physical properties observed when matter approaches the quantum domain.][2] Specific properties of nano-materials such as reflectance, absorption, conductivity, molecular geometry and mechanical strength can take on strange and often advantageous variations as compared to there bulk or macro-sized counterparts.[3] Such variations are related to quantum phenomena when material dimensions approach the characteristic length scales associated with for example the electron mean free path, de Broglie wavelength, exciton Bohr radius or probabilistic band gap.[4]

However if Feynman were to return today he might be a bit disenchanted with the level of advancement in nanotechnology achieved thus far. Certainly there have been tremendous advancements particularly in computer chips and processing technologies as our everyday devices become ever more powerful and compact. Nanoimprinting via photolithography has made logic densities on the order of millions of transistors per millimeter squared a reality, and the technological revolution spreading from silicon valley across the world has changed our lives forever. And yet much of the technology in use today remains in the micro-electronic state, orders of magnitude larger than Feynman's nano-vision.

The principal reason for this short fall is the methodology associated with modern nano-fabrication, which until recently has been dominated by top-down approaches including serial e-beam lithography and chemical etching.[5] And though these methods have rendered much of the integrated circuit technology we rely on today, they face lim-

itations on the smallest length scales and highest material aspect resolutions. An alternative methodology termed bottom-up nano-fabrication involves the spontaneous generation and self-assembly of complex nanostructures resulting from manipulation of a materials environment rather mechanical interaction with a materials interface.[3] This hands-off approach can be realized through a number of techniques including colodial solution deposition, chemical vapor deposition and anodic oxidation of various metals.[4] In this work we focus on the anodic oxidation approach because of its potential for uniformity over large domains and the relatively high degree of control over the resulting nanostructures.[6]

Anodic oxidation of metals, otherwise known as anodization, is a process by which the metal in question is intentionally oxidized via an electrochemical reaction. The sample to be oxidized is connected to the anode, or positive side of a DC power source, while a sample of similar characteristics is attached to the cathode or negative side of the same power source. Both leads are then immersed in an acidic solution called the electrolyte and a current is passed between them. Figure 1.1 details this setup.

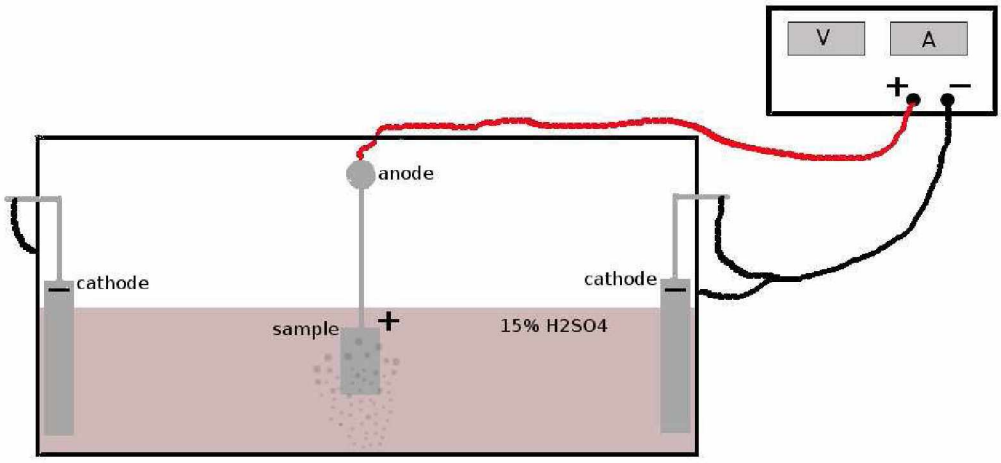

Figure 1.1. Typical anodization setup. The aluminum sample serves as the anode connected to the positive side of a DC power supply. Cathode material varies but must be conductive and generally resistant to acids.

Certain metals such as aluminum or titanium anodized in this way form a porous oxide barrier, the characteristics of which are dependent on the anodization parameters includ-

ing the type of acid employed as the electrolyte, pH of the electrolyte, applied voltage, temperature and current density. Under specific conditions the oxide formed can exhibit highly ordered cylindrical nanopores uniformly distributed in a hexagonal pattern.[7] For example, a piece of Al anodized in oxalic acid with an applied voltage of $40V$ will exhibit such a porous oxide within a number of hours. However the same sample anodized at a voltage say $\pm 10V$ or more from this optimum value will exhibit a much lesser degree of uniformity if at all.[8] And the oxide may in fact become amorphous, wherein the nanopores assume random distributions, orientations and even variable sizes. Let us discuss now the principal mechanisms underlying this behavior.

1.1 Theory

Although there is no universal agreement amongst the scientific community as to the theoretical reasoning governing self-assembly of nanopores, there are essentially two principal factors at work which serve to explain the process by which this porous oxide forms, and why at certain voltages it forms into a highly ordered array of uniform nanopores. The former happens as a result of field assisted dissolution and the latter is due to the rate of volume expansion.

Field assisted dissolution theory was described by O'Sullivan and Wood [9] in the late 60's with a paper generally considered to be a classic work in the area of porous alumina and is cited in the vast majority of subsequent research. The electrochemical reaction describing the oxide formation is given by

$$2Al + 3H_2O \Longrightarrow Al_2O_3 + 3H_2 \quad [\Delta G = -8.65x10^5 J], \tag{1.1}$$

where ΔG is the Gibbs energy change.[4] Oxide growth occurs within a barrier layer at the aluminum surface and the process continues so long as the barrier remains electrically transparent. Al^{3+} ions liberated from the aluminum substrate migrate into the barrier layer to combine with OH^- and O_2^- ions from the electrolyte.[4] As new oxide is formed at the pore bottoms a thin film of alumina begins to grow out of the barrier layer in a direction normal to the aluminum surface. Initially the barrier formation is fairly chaotic but within the first few minutes of anodiztion the system maintains a steady state oxide production.

At the same time new oxide is forming within the barrier layer the process of field assisted dissolution is eroding the oxide within the space of the pore bottom there by maintaining the closed circuit anodization process. In this way, oxide continues to form in a porous array, otherwise the process would fail as alumina is poorly conductive. O'Sullivan and Wood maintained that this dissolution process involved the stretching and breaking of aluminum-oxygen bonds under the applied electric field which is concentrated at the pore bottoms.[3] The weakened bonds translates to a reduced effective activation energy for dissolution which destroys the oxide in these concentrated regions.[9] Although it has not been measured it is proposed that significant joule heating at the pore bottoms would also contribute to a thermally enhanced dissolution of oxide.[9] It should also be noted that though O'Sullivan and Wood's model is widely accepted, by their own admission it is not possible to quantify field assisted dissolution theory until the reaction rate on a planar surface could be measured or the field at the pore bottom estimated from the resulting geometry.[3] A difficult task which to date remains unaccomplished.

Amorphous aluminum oxide can be produced over a wide range of applied voltages and it is this type of oxide that is used extensively in industry for corrosion resistance. In this case the principal need is for a nanoporous surface capable of accepting various dyes or sealants, as for example the brightly colored aluminum carabiners used for rock climbing and key chains. Because the dye and clear coat penetrate the porous oxide surface it is effectively embedded in the oxide making for an extremely durable surface as opposed to a thin layer painted over a surface which can be worn away with use.

However, for very narrow ranges of applied voltage specific to the organic acid serving as the electrolyte, the oxide can assume a highly ordered distribution of hexagonally arranged nanopores having a uniform shape and size.[10] The reason for this has to do with the volume expansion of oxide during the anodization process. The rate of oxide production is dependent on the applied voltage with the charge transfer carried by the Al^{3+} ions liberated form the aluminum substrate serving as the anode.[8] However not every Al^{3+} ion liberated contributes to the resulting oxide as a percentage are lost to the electrolyte via field assisted dissolution. These ions actually result in a dark metallic film which accumulates on the cathode over time. Thus we can define the overall current efficiency as the ratio of the volume of Al_2O_3 formed to the total volume of Al consumed.[11]

Now the atomic density of Al within Al_2O_3 is a factor two lower than that of metallic Al, thus a current efficiency of 100% would correspond to an expansion of alumina during oxidation to twice the original volume.[11] Of course there would be some reductions due to cation incorporation and under normal experimental conditions the expansion is indeed less than twice the original volume. Jessensky et al [8] performed a detailed analysis of volume expansion and found that the optimal conditions for the formation of ordered structures occurred for current efficiencies corresponding to a moderate volume expansion during anodization. In oxalic acid this turned out to be a current efficiency of $\sim 55\%$ which occurred at $40V$.[8] At an applied voltage of 30 and $60V$ the volume expansion was found to be 45 and 65%, respectively, with noticeable degradation of pore uniformity.[8] Similar optimal conditions have been reported for anodization in sulfuric acid at $25V$, in phosphoric acid at $160V$, and in malonic acid at $240V$.[3]

The relationship between field assisted dissolution and the rate of volume expansion is governed by the applied voltage which in-turn effects the current density j given by

$$j = Aexp\left(\frac{\beta V}{d}\right), \tag{1.2}$$

where A and β are material-dependent constants, V is the applied voltage, and d is the effective distance across the barrier layer.[12] It has been shown that the rate of volume expansion increases with the applied voltage, however it is thought that the reaction rate for field assisted dissolution also increases resulting in an increased porosity of the oxide.

Under optimal conditions, the self-ordering of the pores themselves is always hexagonal. Although there are proposed explanations for this fact including mechanical stress, crystal formation and opposing inter-pore forces, there has yet to be a definitive answer and likely the hexagonal distribution is a result of multiple factors. Nevertheless, in the case of self-ordered porous alumina the size and distribution of the pores is uniform. The porosity P of a hexagonal distribution can be expressed mathematically as

$$P = \frac{2\pi}{\sqrt{3}}\left(\frac{r}{D}\right)^2 \tag{1.3}$$

where r is the pore radius and D the inter-pore distance. Nielsch et al proposed the 10% porosity rule, which states that the optimum porosity for uniform self-ordering is

10% regardless of the electrolyte. This is because r and D remain constant for a uniform distribution.[11]

However, field assisted dissolution also depends on the pH of the electrolyte such that a lower pH, which describes a stronger acid, will yield smaller pores.[3] Thus one can produce an increased or decreased density of pores within the optimal conditions dictated by the rate of volume expansion and the 10% rule by incorporating a stronger or weaker concentration of a given electrolyte. The end result is an experimental method by which highly ordered nanoporous thin film oxides can be produced via a bottom-up approach. This self-assembled nanoporous oxide in turn serves as an ideal template for the fabrication of various nanostructures including quantum dots, nanorods and nanotubes. Aluminum served as the anode material for this work because of its relatively low cost and the extensive body of previous works investigating nanofabrication via anodized aluminum.

1.2 Previous Work

The anodization of aluminum for corrosion resistance and material strength has been an industry standard since the 1920s; however the observation of aluminum oxide as a means of nanofabrication was first reported on by Masuda et al out of Japan in the mid 90's. In this and subsequent work a technique was developed called two-step anodization in which a pre-treated aluminum sample is anodized at relatively low current densities for up to 160 hours.[7] The oxide is then dissolved away in a separate bath and the sample is reanodized under the same conditions.[13] The resulting oxide was found to exhibit highly ordered nanopores uniformly distributed in a hexagonal pattern.[14]

Referring to Figure 1.2 we can identify the basic structure and material characteristics of porous anodic alumina (PAA), which is the term used to describe uniformly distributed nanoporous oxide templates formed by anodizing aluminum. In the first minutes of anodization a barrier layer is formed on the aluminum surface through which Al atoms migrate to combine with oxygen atoms forming alumina. The anodization process will continue provided the barrier layer remains electrically transparent.

The thickness of the barrier layer is given by $t_{barrier}$. The pore diameter D_p and the interpore distance D_{int} can be seen as well.[15] It is worth noting that D_{int} is sometimes refereed to as the lattice constant. The wall thickness between pores, t_{wall}, can be a point

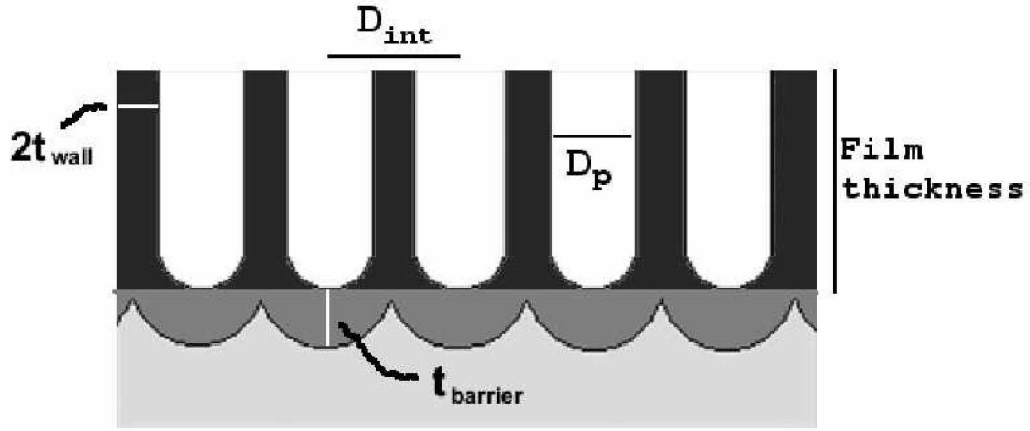

Figure 1.2. Characteristic definitions for PAA. These definitions are used extensively in the literature to describe PAA properties.[8]

of confusion as some reports prefer the convention $2t_{wall}$ thereby attributing one t_{wall} to each pore of a neighboring pair. This is further complicated by the wall structure itself with is comprised of an inner an outer layer as seen in Figure 1.3. The layer interior to the pores which appears darker upon imaging consists of a dense pure alumina. Where as the brighter outer layer comprising the actual pore wall is cation-contaminated.[3]

This gives rise to another parameter called the inner wall thickness t_{inner}. All of these parameters are typically given in nanometers with the exception of film thickness which is generally on the order of tens to hundreds of microns. The ratio of surface area occupied by nanopores and the alumina walls in between is referred to as porosity and for a hexagonal distribution of PAA can be expressed as

$$P = \frac{2\pi}{\sqrt{3}} \left(\frac{D_p}{D_{int}} \right)^2 \tag{1.4}$$

which for optimal self-ordering of nanostructures was previously found to be 10%.[11]

Another point with respect to anodizaiton is the magnitude of the applied potential which dictates the oxide film growth rate. Of the two voltage regimes in the context of PAA, the standard technique developed by Masuda has come to be described as mild anodiztion (MA), having fairly narrow bounds specific to the electrolyte used.[16] MA via sulphuric acid for example is conducted around $25V$. At the industry level however the

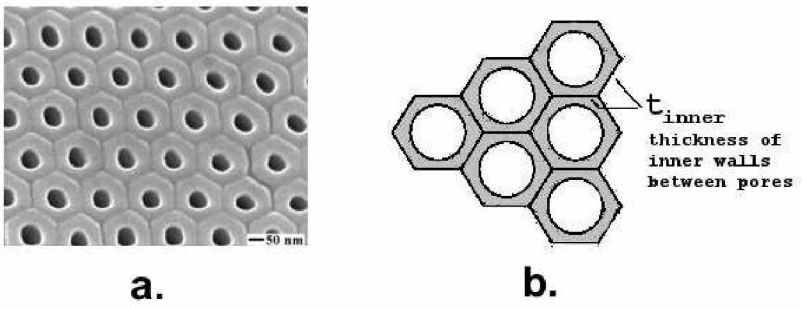

Figure 1.3. Inner and outer pore wall detail. The inner layer interior to the pores is composed of a dense pure alumina, while the brighter outer layer comprising the actual pore wall is less dense owing to ion incorporation.[11]

need is for efficient oxide growth that combines hastened growth rates with the desire for a randomly distributed nanoporous characteristic. In these applications higher voltages are applied in order to accelerate the oxide formation and these regimes are referred to as hard anodization (HA).

Returning to Masuda's original work, after he had refined the two-step anodization technique and could reproduce PAA templates, he proceeded to electrolytically deposit gold into the pores and after dissolving away the aluminum and alumina substrates was left with a nano-templated gold film with notably different optical properties as compared to a bulk or standard gold film. The templeated Au film had a surface comprised of uniform nano-hemispheres or bumps where as the bulk film had a standard polished surface. The templeated film appeared reddish in color and spectral measurements revealed that indeed the reflectance had shifted for wavelengths greater than 450nm.[7] This work became the impetus for a new regime of nanofabrication via the self assembly of metallic oxides.

The two-step anodization technique detailed in Figure 1.4 was subsequently employed as the traditional method where by researches explored numerous additional variations and there effects on nanofabrication including various electrolytes, cathode materials, temperature regimes, current densities and sample preparations. After a decade or so of addi-

tional work it was fairly well accepted that the nanopores themselves remained cylindrical in geometry across a wide range of experimental variables, even as D_p, D_{int} and the porosity might vary significantly. This constant feature of symmetrical, cylindrical pores offered a multitude of post-processing nano-fabrication possibilities including nanotube construction, stimulated growth of nanowires and pattern transfer technologies. However it has been demonstrated in recent years that material properties due to quantum confinement are dependent on both size and geometry, making it desirable to control both aspects in the context of nano-fabrication. Regarding anodized aluminum the question becomes one of altering the geometry of the inherently cylindrical nanopores while retaining the uniform distributions and self-assembly of the oxide.

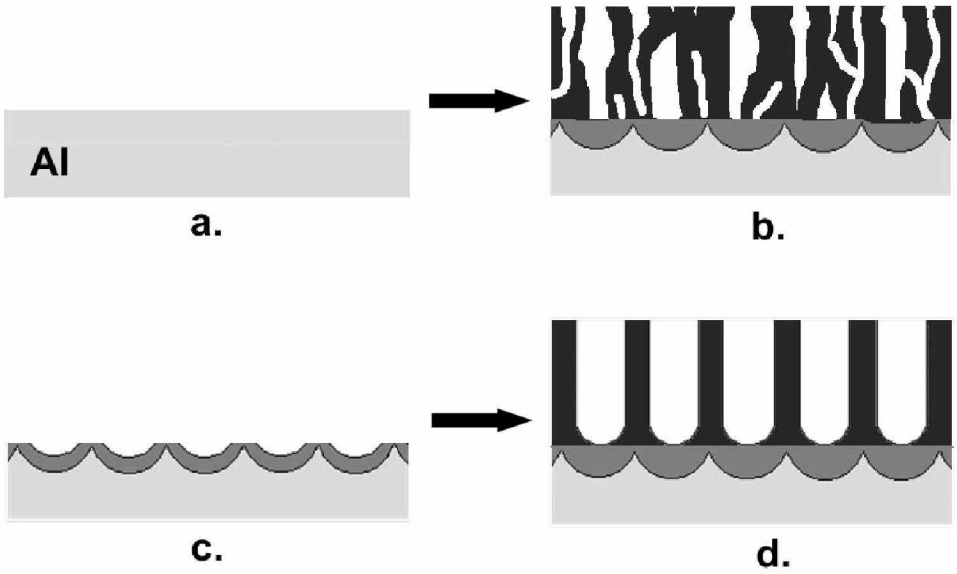

Figure 1.4. Two-step anodization technique. a. A polished aluminum substrate. b. Anodization under MA conditions for an extended period of time resulting in a somewhat amorphous oxide film. c. This film is then striped away in a separate acid exposing a scalloped surface on the aluminum substrate. d. Reanodization under the same MA conditions now with preferential pore formation over the existing surface resulting in a uniform distribution of self-ordered nanopores.[7]

Within the area of pore-texture engineering there has been work done over the last five years or so related to post processing alterations, preprocessing treatments and exper-

imental variations to the traditional two step anodization method. Krishnan [3] explored a method in his 2005 MIT thesis where the electrolyte was changed out partway through the second andoization step resulting in a change in the pore diameter roughly halfway trough the oxide thickness. Specifically the pore diameter decreased form 85nm to 55nm when the electrolyte was changed from phosphoric acid to oxalic acid.[3] He postulated that additional variations to the electrolyte with increased frequency could result in pore profiles having conical geometries termed nanofunnels.

Nagaura et al [17] developed a method where the traditional nanoporous oxide was chemically etched to widen the pores and then reanodized under similar conditions. This resulted in a tapered pore profile having a somewhat two-step or tiered geometry. Repeated applications of the anodizing, etching, anodizing procedure up to five times eventually resulted in nanopores that where uniformly conical in shape having base diameters of around 100nm.[18] This geometry afforded a new descriptive parameter for PAA called the aspect ratio which is simply the ratio of a cones total length to is maximum diameter. Figure 1.5 provides a comparative example.

Nagaura et al extended this pore widening/reanodization method to produce conically profiled nanoporous alumina templates of varying aspect ratios from 1.0 up to 3.25. The top diameter remained approximately 100nm however the oxide thickness was increased resulting in a taller more slender nanocone. One can see that in terms of deposition and templating a lower aspect ratio is desirable for complete pore incorporation. Nagura proceeded to fill the 1.0 aspect ratio conical nanopores with nickel via electrolysis deposition as seen in Figure 1.6.[17] This is a good illustration of how nanoporous alumina templates can be used to fabricate secondary nanostructures via deposition.

Yamauchi et al [19] employed this technique to fabricate conical PAA which where subsequently spin coated with a precursor solution used in the generation of self organizing mesoporous channels to investigate the channel orientation properties. Surprisingly they found that the difference in aspect ratios translated to a difference in mesochannel orientation. The orientation of mesochannels depends on the orientation of mesopores produced by the self organization of surfactants and inorganic species comprising the precursor solution which occurs during the spin coating process. Within the low aspect ratio nanofunnels, the mesopores took on a random distribution resulting in a perpendicular

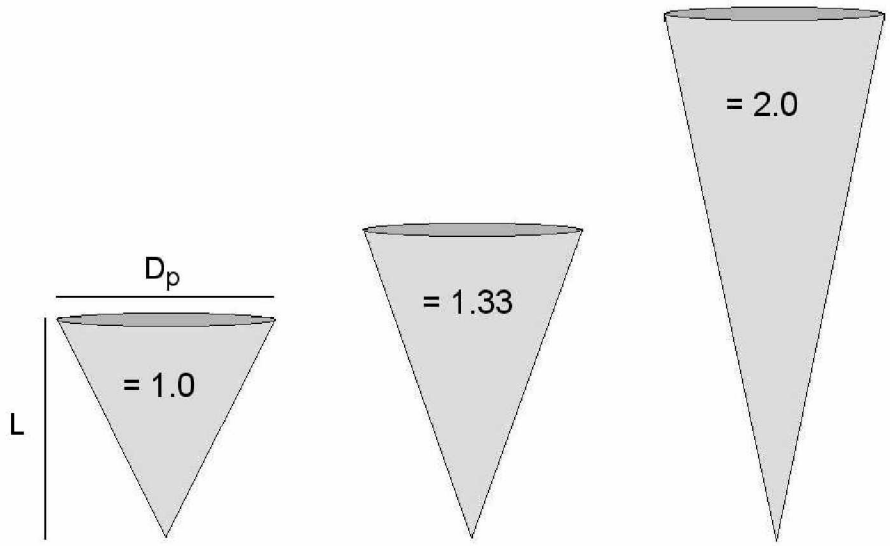

Figure 1.5. Details of aspect ratio. The aspect ratio increases with increasing film thickness however it becomes more difficult to incorporate the full pore volume with deposition of secondary materials.

orientation of mesochannels as they grew vertically upwards form the PAA.[20] Though this orientation had been previously generated by other methods, what had not yet been successfully realized was the fabrication of mesochannels oriented parallel to the inducing substrate. When Yamauchi applied the same process to high aspect ratio nanocones the mesopores took on an ordered distribution of vertically stacked donut-like structures within the nanocones which resulted in mesochannels oriented parallel to the substrate as seen in Figure 1.7.[20] This new class of films holds great potential for future applications such as nano-filtration and represents another example of complex nanofabricaiton via PAA.

Of course one draw back to post-processing fabrication techniques such as etching is the resulting increase in pore diameter. If the subsequent application requires a specific volume regime and geometry then one might sacrifice pore diameter in pursuit of pore profile when employing a widening method. This particular draw back suggests investigation of in-process tailoring techniques which can affect pore profile and distribution as a

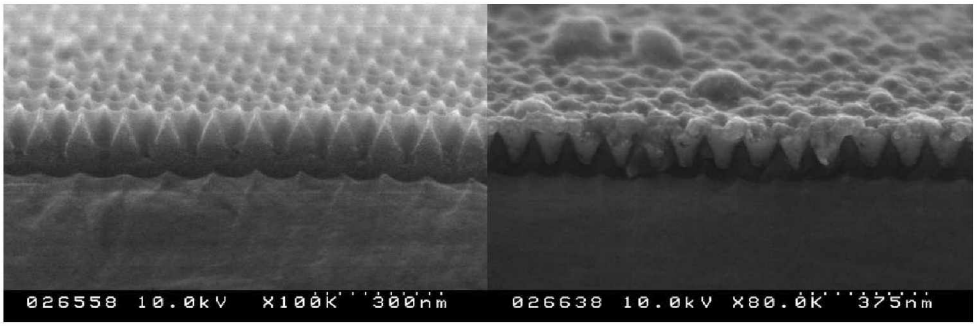

Figure 1.6. Nickel nanocones via deposition on PAA. The nanocones had an aspect ratio of 1.0 allowing for total pore incorporation via electroless deposition.[17]

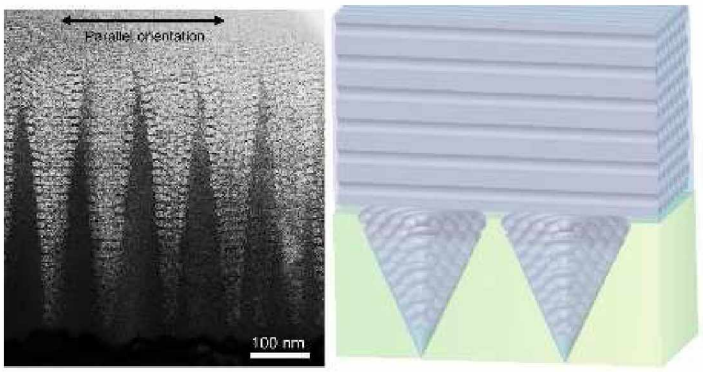

Figure 1.7. Parallel orientation of mesochannels on conical PAA. TEM image of mesochannels on across PAA nanocones filled with stacked deposits of mesopores.(left) Illustration of this nanostructure.(right)[20]

matter of anodizing variables. It has been known for quite some time that of the three main electrolytes: sulfuric, oxalic and phosphoric acids, the resulting pore diameter increases from 25nm through 200nm respectively.[20] And it was previously stated that Krishnan et al used this fact to produce nanofunnels by changing the electrolyte part way through the anodization process. However this method is somewhat restrictive on the through put efficiency of PAA nanofabrication and may introduce cross-contamination effects regrading the mechanical stability of the resulting oxide. This further suggests examination of the applied voltage and current densities which drive the electrochemical reaction as a possible mechanism for in-process tailoring of PAA geometries.

That idea brings us to the most recent works on nanofabrication via PAA in which variations to the traditional two step method have been developed specifically for investigation of the pore profile and controlled structural engineering of the 3D pore geometry. In the literature Lee et al [21] is the first to report on a combination of MA and HA into a single process and to characterize the effects. The principal difference between the MA and HA regimes is the magnitude of the current density j observed in the system which is a function of the potential drop between anode and cathode.[22] For MA, a steady drop of say 40V in the case of oxalic acid yields current densities on the order of $5mAcm^{-2}$.[3] Additionally this value will remain fairly constant through out the experiment once the barrier layer at the pore bottom has formed and stabilized after the first few minutes of anodization. In the HA regime potentials of $110-140V$ yield current densities on the order of $200-300mAcm^{-2}$, which are observed to decrease exponentially from the maximum value achieved upon barrier layer formation.[21] Numerous oxide characteristics are altered in the HA regime including an increased growth rate, reduced porosity, increased D_{int} and increased D_p. However due to significant joule heating at the substrate interface this technique must be conducted at reduced electrolyte temperatures in the range of $0-10C$.[12]

Upon combination of MA and HA techniques Lee et al observed pore diameter modulation owing to the regime character differences described above. Specifically the resulting oxides were formed by a technique called pulse anodization conducted with sulphuric acid. In this experiment the steady MA at 25V was incrementally pulsed with HA conditions at 35V for $0.1s$ with a period of $180s$ for a total experiment length of 150 minutes.[21] The resulting pore profile exhibited periodic modulation of diameter with the MA segments roughly five times the length of HA segments. This configuration resulted in a slabbed oxide as seen in Figure 1.8 from one of Lee's publications.

Interestingly it was found that the crystalline fracture modes differed between the MA and HA layers. In order to obtain SEM micrograph images of the pore profile, samples are mechanically fractured by bending in order to crack the oxide there by exposing the vertical pore profiles. Lee found that the difference in fracture modes created stair step cracks in HA versus a typical straight walled vertical fracture through the oxide thickness associated with MA. The HA slabs tended to fracture along the pore boundaries where as the MA oxide tends to break along the pores themselves.[21]

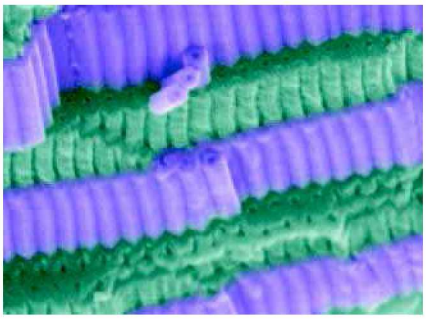

Figure 1.8. Slabbed layering of alumina via pulse anodization. False coloring of the image helps distinguish the alternating layers of MA and HA nanopores.[21]

Additionally it was observed that the porosity of the HA-PAAs varied as compared to MA-PAAs depending on the electrolyte. In oxalic acid the HA-PAA porosity was seen to be about 30% less than in MA-PAA, where as sulfuric acid resulted in a greater HA-PAA porosity.[21] The reduced porosity from HA in oxalic acid is possibly attributed to enhanced proton activity at the pore bottom with significant joule heating from the high electric field. On the other hand the increased porosity associated with HA in sulfuric acid is attributed to a much higher incidence of anionic impurities, mostly sulfur dioxide in the PAA, about 88% greater than MA according to tunneling electron microscope-energy dispersive x-ray spectroscopic analysis.[21] Local chemical dissolution of the pore walls by electrolyte during HA would be greater in the impure PAA as compared to the relatively pure MA-PAA. This periodic zone of etch vulnerable HA-PAA through the thickness of the thin film allowed for directed dissolution of the HA layers resulting in columnated sheets of MA/HA-PAA as seen in Figure 1.9.

This brings us to the most recent report on modified anodization techniques related to PAA by Losic et al termed Cyclic Anodization. Once again we have a combination of MA and HA regimes but the anodizaiton conditions are varied in a slow oscillatory manor by changing the profile, amplitude and period of the current signal.[23] Although this method was applied to the three principal electrolytes they report primarily on the results obtained via phosphoric acid because the pore dimensions are on the micron scale making SEM analysis easier. The driving experimental control in this work was the oscillatory current density applied to the anodization process. Under steady state voltage conditions the

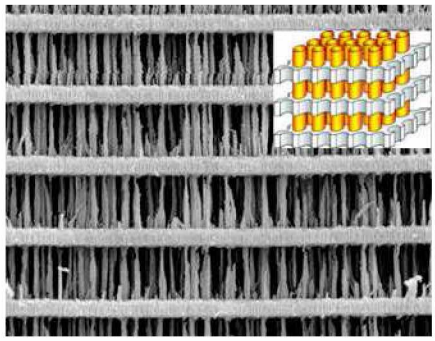

Figure 1.9. Columnar layering of MA and HA PAA. The increased susceptibility of the HA layers to wet etching results in colunmated nanostructures. The inset shows an idealized version of the internal structure.[21]

anodization current density follows a well known curve in time characterized by an initial and steep increase in magnitude up to a maximum value followed by a gradual decrease as the barrier layer thickness increases. Figure 1.10 details this steady state condition for an experiment conducted in oxalic acid.

However Losic et al [23], using a PC-controlled power supply, forced the anodization current density into a sawtooth pattern casing the voltage to fluctuate between the MA and HA regimes which for phosphoric acid where about 80 and 160V respectively.[23] This transition occurred more slowly than the pulse anodiztion method with a single cycle encompassing roughly one minute. This cycle was subsequently repeated for a total experiment length of about 12 minutes.[23] Figure 1.11 provides voltage and current profiles along with SEM images of the resulting oxide pore profiles. Losic et al termed the new anodization regime between MA and HA as Transitional mode or Transitional Andoization (TA).[23] From the figure it is apparent that this region of an exponentially increasing current density results in a conical pore profile with the diameter gradually increasing along with the current density. This periodic modulation of pore geometry is repeated along the pore length through the oxide film thickness.

Losic et al proceed further to modulate the current signal amplitude as well as the form and frequency including sinusoidal, triangular, square and combination signals to achieve nano-sculpting of the pore profiles.[23] In each case the modulations in pore geometry observed via SEM analysis where attributed to the corresponding current density profile

Figure 1.10. Steady state voltage and current profile. This data was recorded from an experiment in oxalic acid. The voltage was held constant at 32V, while the current density is seen to rapidly obtain a maximum before slowly decreasing. Total experiment length is 12 minutes.

with a general correlation between increased pore diameter and increasing current density. It should be noted however that the MA regime for anodization in phosphoric acid is cited as 160V in the majority of peer-reviewed works on the subject. Losic et al do not address this fact and thus it is uncertain as to which voltage regime their experiment is occupying. They state that anodization parameters had to be carefully considered in lue of the cyclic nature of the current density and indeed optimal conditions included a 0.1 molar phosphoric acid electrolyte chilled to $-1C$.[23] Never the less their work establishes a clear relation between pore geometry and current density as can be observed in Figure 1.12.

1.3 Goal of this Work

The goal of this work is to investigate the effects of a varied potential difference on the anodization process. Specifically to affect a self-assembled conical pore profile by changing the applied voltage in time. From previous work we have seen that conical pore profiles can be realized via post-processing techniques such as directed wet etching and multi-step anodization. However in these processes the pore dimensions generally increased by an order of magnitude or more. We have also seen that galvanostatic or current variations via

cyclic anodiation directly effected the resulting pore profiles, but to date there has not been a reported investigation of potentiostatic or voltage variation on the anodization process. Although Losic et al [23] mention briefly of attempting potentiostatic variation they abandoned this avenue in favor of galvanostatic citing experimental inconsistencies. In this regard our idea is not entirely novel however to our knowledge it has not been previously investigated in detail either.

We strive to realize a conical pore profile in process with the traditional two-step anodization method while maintaining the smallest pore dimensions possible. Pores having diameters below 20nm with aspect ratios about 1.0 would be ideal as those dimensions would be much closer to some of the characteristic lengths governing the quantum confined spatial domain which Feynman eluded to so many years ago. Thus we set out to answer the question of what effect a time varied potential difference will have on the traditional two-step anodization method, a technique we refer to as *variational anodization*, and if in fact conically profiled nanopores can be realized via such a technique.

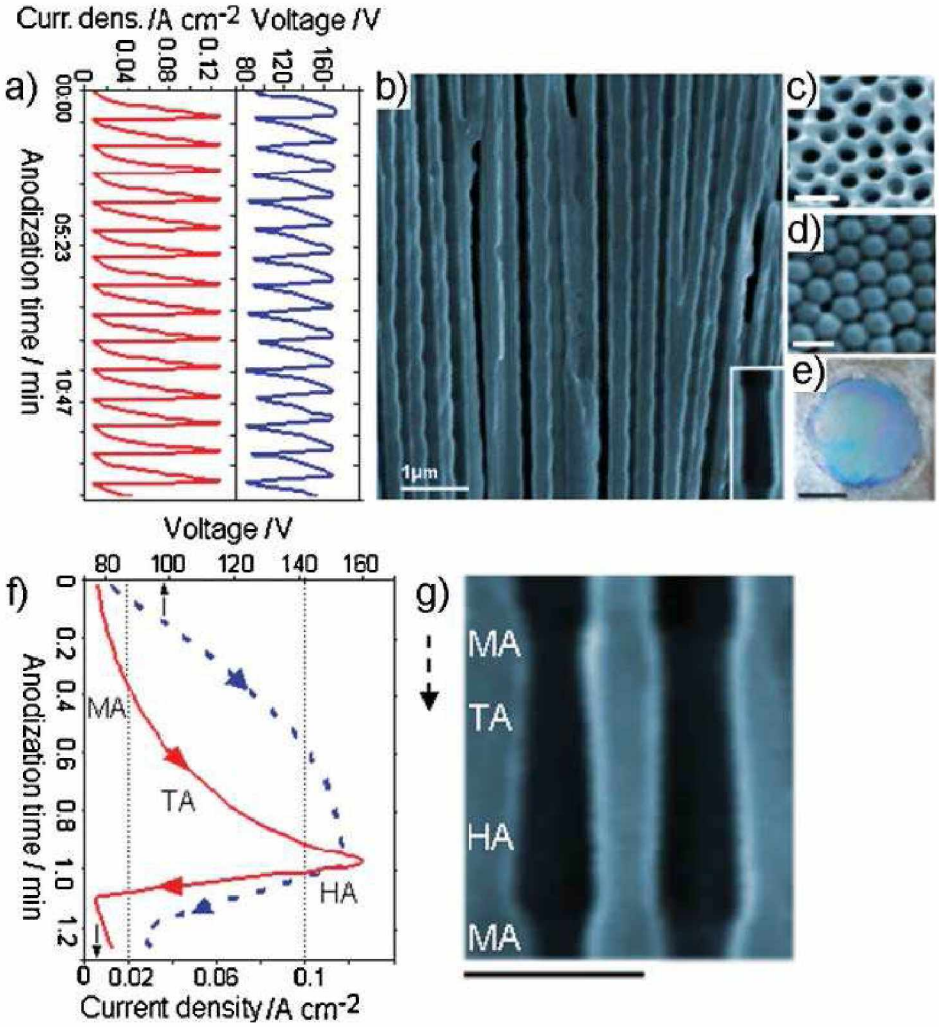

Figure 1.11. Voltage, current and SEM micro-graphs of cyclic anodization. (a) Sawtooth current profile resulting in periodic fluctuation of applied voltage between MA and HA regimes. (b) SEM image of modulated pore geometry, (c-d) SEM images of top and bottom of oxide film showing hexagonal ordering of pores, (e) digital photograph of thin film sample showing iridescence, (f-g) and current/voltage profiles for one cycle along with SEM image of subsequent pore modulation with anodization regimes labeled along pore length.[23]

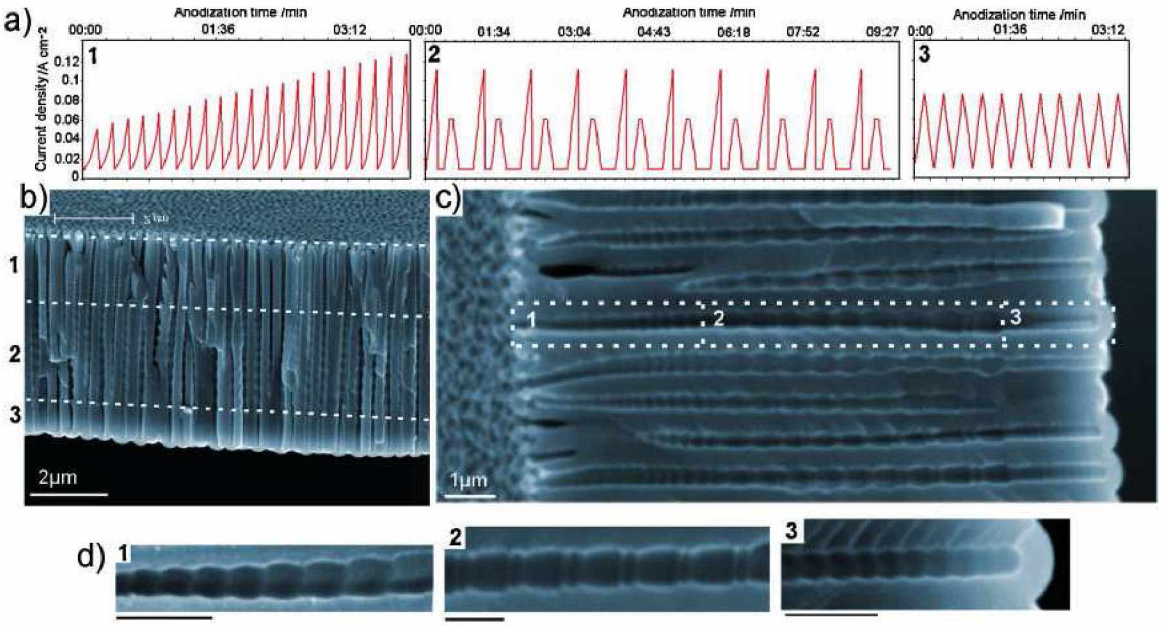

Figure 1.12. Current and pore profiles of combination cyclic anodization. (a) Combination current signals beginning with linearly increasing amplitude triangle wave (1), modulated amplitude triangle wave (2) and standard sawtooth wave (3). (b-d) SEM images of resulting pore profile owing to the variational current profiles given in (1-3).[23]

Chapter 2
Experimental Procedure

The principal difference of variational anodization with respect to the traditional two-step anodization technique is the application of a time dependent potential difference during the second anodization step. Effecting this change linearly necessitates incorporation of a computer controlled DC power supply which can be programmed to produce a specific voltage-time curve. A system having such a power supply could then anodize one sample at a time but do so with reproducible operating conditions. The applied voltage then serves as the experimental control with time as the independent variable. Numerous time varied voltage programs could be written and applied to a common starting sample condition such that any subsequent differences could be quantified and attributed to the experimental control. The principal reporting mechanisms in such an investigation are then the voltage and current profiles in time along with Scanning Electron Microscopy (SEM) analysis describing the subsequent nanopore profile and thin film characteristics. To our knowledge such an investigation has not been previously executed.

2.1 Materials

As was previously mentioned the principal components of a typical anodization set up include a DC power supply, cathode, electrolyte and in this case the capacity to record voltage and current values in real time. The anode is the sample itself exposed to the electrolyte in a corrosion resistant vessel thereby completing the circuit. We shall discuss these materials individually and, where appropriate, in the context of an evolution in experimental technique as problems where identified and remedied over the course of this work.

Although the literature regarding nanofabrication via anodized aluminum is thorough with respect to experimental parameters, very little is provided regrading the logistical or applicatory means by which the experiments are conducted. Particularly with respect to containment, which must be multi-functional allowing access for measurement of various experimental parameters while also securely maintaining the hazardous and highly corrosive organic acids comprising the electrolyte. Further more, as indicated by equation 1.1, the principal by product of the electrochemical reaction aside from aluminum oxide is hy-

drogen gas. This gas is produced quickly and if not properly vented the induced pressure will breach the containment security of the vessel resulting in acidic leaks. All of these factors combined make the design and implementation of an anodization bath a non-trivial matter.

That being said, the initial design for this work was adapted from a do-it-yourself home anodization booklet self-published by Ron Newman.[24] The setups and techniques described in this guide are intended principally for corrosion resistance and decorative finishing of automotive parts, gun accessories, tools, motorcycle parts and whatever else the home-brew anodizer would be interested in. As such, the anodization is of the industrial type with large open baths operating at higher voltages able to accommodate multiple large sized anodes. However the basic requirements of a corrosion resistant vessel such as polyurethane or polypropylene, various cathode materials such as aluminum, lead or stainless steel, and the general procedure for preparing samples to be anodized served as the starting point for our work.[24]

Before detailing the experimental setup incorporated to perform this research it should be noted that this work has never been supported through external funding. Most of the materials needed were either borrowed from the physics department, checked out of surplus, donated by the chemistry department or paid for out of pocket. With this budgetary restriction on design and fabrication the adaptation or re-purposing of common and cost effective materials was a priority. Though some of the following descriptions may seem amateurish to the more senior experimentalist, the work is nevertheless sincere and was carried out to the best of our ability given the circumstances.

The initial anodization setup used a modified high density polyethylene single gallon water jug commonly available from various retailers. A bus bar made of 6063 Al rod from Home Depot spanned the width of the tank from which the anode was suspended using sample holders made from Al welding rod. 6063 Al is a low grade Al but was readily available and affordable. The cathodes were also made from this material in plate form with one placed at each end of the tank. A 200V DC power supply already in the lab provided power but could not be varied consistently in real time; thus the initial goal was to try to reproduce cylindrical nanopores via the traditional two-step anodization method.

Sulfuric acid was chosen as the electrolyte because UAF HAZMAT donated 2.5L of

lab grade 95% redox H_2SO_4 in an open botte that had been sitting in their store house for some time. Through out the literature Al samples used for anodization are always of a very pure grade, exceeding 99.99% Al, and typically available in thin foil form or wafer form from supply companies such as AlfaAesar. However this metal is fairly expensive and was initially unavailable to us. As a result initial samples were cut and polished from the 6063 Al to test the setup and refine the operating parameters.

Early runs produced anodized aluminum using $0.3M$ sulfuric acid. Samples were then etched in phosphoric and chromic acid borrowed from the chemistry department and re-anodized as per the two-step procedure. Samples were then analyzed using the Advanced Instrument Laboratories (AIL) SEM. Though the system worked in the sense that aluminum samples where anodized, the oxide produced was of the amorphous type distinguished by large surface pitting and cracking associated with a general non-uniformity as can be seen in Figure 2.1. Of course this type of surface oxide was mostly owning to the rough nature of the initial sample condition as well as to alloying elements in the metal such as Ni, Fe, and Si, which react differently under such electrochemical conditions than does Al.

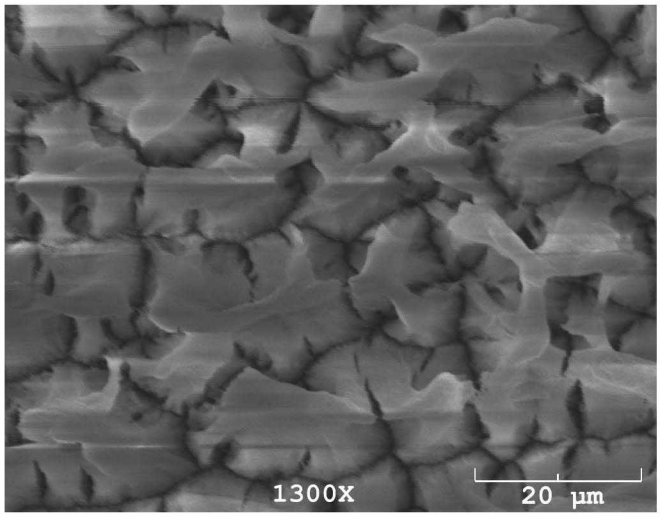

Figure 2.1. SEM image of amorphous aluminum oxide. The surface is characterized by a varying degree of pitting and cracking.

We attempted to improve the rough surface nature of the 6063 Al by mechanical pol-

ishing to a mirror like finish as can be seen in Figure 2.2. A few reports in the literature detailed sample preparation conditions and parameters required for the formation of nanostructures. They reported surface qualities having average roughness measurements of less than 10nm via Atomic Force Microscopy (AFM).[25] AFM analysis was performed on our samples before and after mechanical polishing and though a drastic improvement was seen as detailed in Figure 2.3a and b, the surface quality remained insufficient with roughness averages of 50nm or more. This condition would necessitate the eventual design and implementation of an electropolishing technique were in the high points or peaks of an exposed surface are dissolved away more rapidly than the surrounding area as the electric field is concentrated on those points.

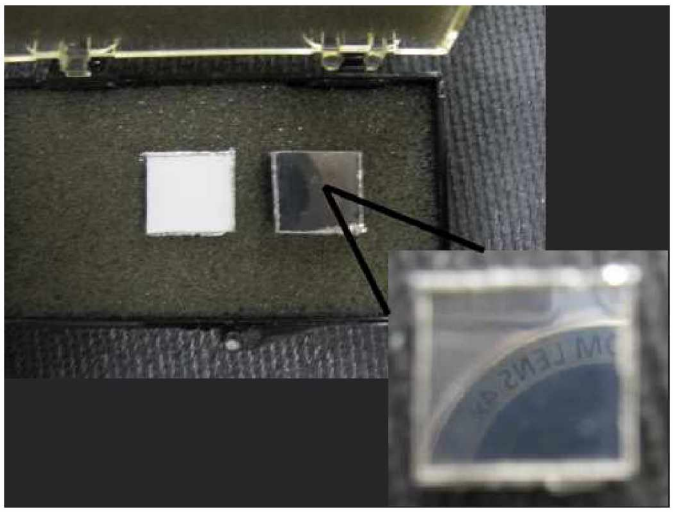

Figure 2.2. Mechanical polishing. Samples cut from 6063 Al were polished to a mirror like finish prior to anodization.

Nevertheless, samples having been mechanically polished to a mirror finish were anodized and the resulting oxide displayed a more porous character with features of various size and distribution as seen in Figure 2.4. This was encouraging and suggested that upon the eventual receipt of a high purity Al foil a process could be developed under which uniformly porous oxide growth could be stimulated.

However along with the initial struggle to reconcile surface quality and the continued production of amorphous oxide films it was also observed that the open circuit voltage of the system was too low. Even with the DC power supply set to 25V the measured

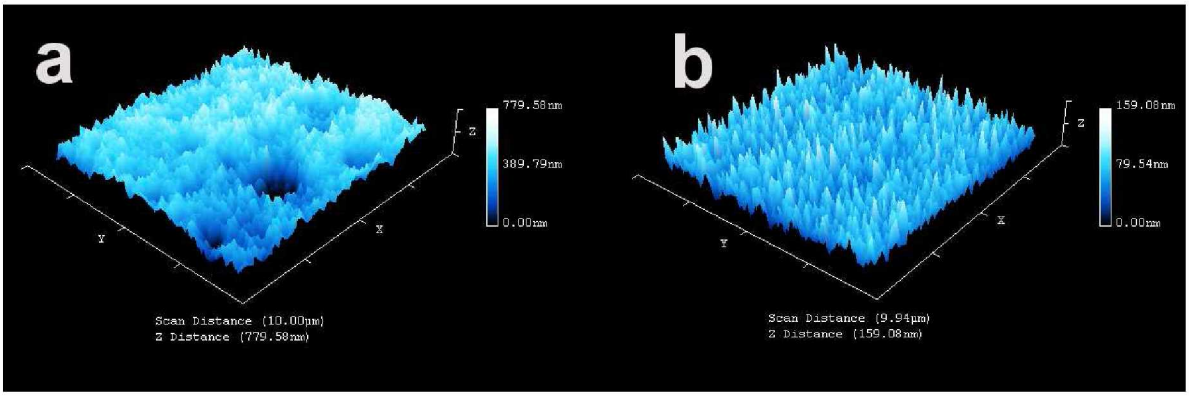

Figure 2.3. AFM analysis of surface quality. a) AFM scan of raw sample. b) AFM scan of polished sample.

voltage was found to vary from $1-5$+V. This indicated that the system resistance was far to high, a result of the excess spacing between cathode and anode within the tank. The current density range for nanofabrication via two-step anodization is generally reported to be on the order of 0.5 to $100 mA cm^{-2}$.[3] Increasing the moality of the electrolyte could lower the system resistance by providing more ions for conduction, but this range again was reported to generally be from 0.1 to 0.6M, and initially our electrolyte was mixed to 0.3M. Though the voltages were low the current densities and pH levels were in the proper range for uniform self assembly of nanopores.

Another issue related to excessive system resistance was the cost ineffectiveness of the anodization setup as it relates to the amount of organic acid needed to sustain the experiments. The initial tank made from a modified water jug required upwards of 5 L of distilled water which in turn commanded about 750 mL of sulfuric acid to obtain a molality of 0.3 M. Having only 2.5 L of acid donated from Hazmat, and the high system resistance due to excess spacing between electrodes, it became clear that a new anodization vessel needed to be designed that would be much more cost effective to operate.

The new design, detailed in Figure 2.5, centered around a reduced reaction volume and sample exposure area. A ten foot length of 2" diameter lab grade clear PVC pipe was purchased and 6" sections were cut from this to serve as containment vessels. The base of the tank was fitted with a two inch plumbing union such that samples could be loaded and exposed to the electrolyte. A modified plug in the lower joint was treaded to accept

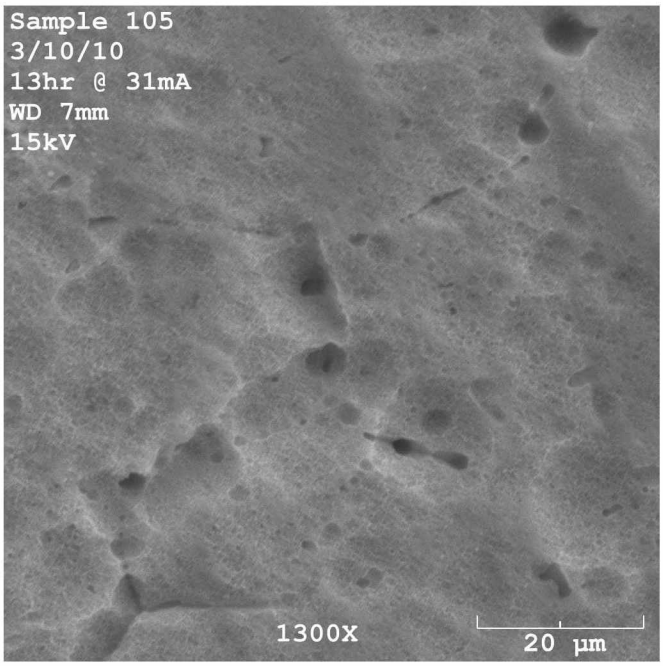

Figure 2.4. Amorphously porous aluminum oxide. Anodizing samples with a polished surface increased the porosity of the resulting oxide.

a $\frac{5}{8}''$ carriage bolt serving as the anode stem upon which thin foil samples backed with a rigid metal coupon were affixed via a small cylindrical magnet recessed into the bolt head.

A second plug glued into the bottom of the containment vessel had a $\frac{1}{4}''$ hole drilled into it with a recessed O-ring on the under side which formed a compression seal against the sample coupons. This resulted in a circular sample exposure area 1 cm in diameter for a total anode area of about 0.8 cm^2. A circular disk of 6063 Al 4 cm in diameter was cut and polished serving as the cathode with a resulting electrode area of about 13 cm^2, well beyond the recommended minimum cathode to anode surface area ratio of $2:1$.[3]

The cathode was fitted to a machined stem of Al welding rod which was secured into a banana jack port drilled into a 2″ plumbing clean-out serving as the top portion of the anodization tank. In this way the interior of the tank could be accessed for service by removing the clean-out, however this was an infrequent occurrence and the clean-out was generally left sealed in place with Teflon tape applied to the threads. In addition to the banana jack port the clean-out was also drilled to accept a length of $\frac{3}{8}''$ polyvinyl tubing

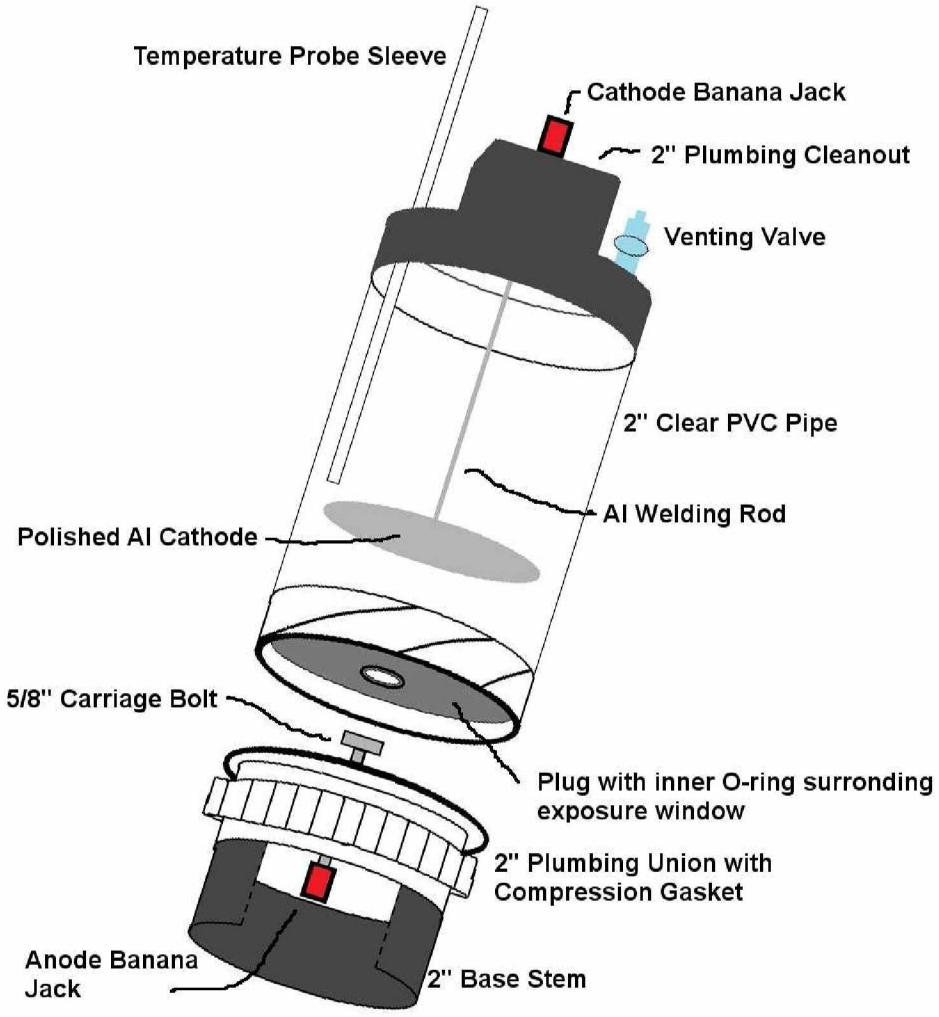

Figure 2.5. Exploded view of redesigned anodization vessel. The design was much more cost effective to operate, requiring about 7mL of sulfuric acid versus 750mL in the original design while also providing greater experimental control.

which served as a protective sleeve for a steel temperature probe inserted to monitor the temperature during reactions, and a thumb screw valve common to aquariums which was used to vent the hydrogen gas during reactions. The whole of the underside of the clean-out with these various modifications in place was thoroughly sealed with pure silicone caulking which remains electrically inert in the presence of organic acids.

The resulting separation distance between anode and cathode was about 5 cm in the new tanks versus roughly 20 cm with the initial anodization tank. System resistances were found to vary between $1-5k\Omega$ for sulfuric based electrolyte and $8-15k\Omega$ for oxalic based electrolyte. The voltage drops in both cases were a solid 25 V and 40 V, respectively, with current densities in the $0.1-50$ mA range. Thus the new anodization tanks successfully satisfied the necessary operational parameters for nanofabircation while providing a safe and secure containment vessel for the experiments.

At this point it became necessary to obtain some of the aforementioned materials to begin the proposed investigation in earnest; and the physics department graciously provided in this respect including a programmable computer controlled DC power supply (P/S) by Quakko, bottles of lab grade phosphoric and chromic acid from VWR and a $100x500x0.25$ mm thick sheet of 99.99% pure aluminum foil from AlfaAesar. A surplused laptop was obtained from surplus upon which a Windows XP operating system was loaded in order to run the programmable P/S software. Additionally a Vernier current probe was purchased to monitor and record the system current profile during anodization.

The voltage signal was the experimental control and was recorded as a function of time by the P/S software. The current probe was interfaced with a LoggerPro device adapter borrowed from the physics department and a free version of Verner's lab software called LoggerLite was installed on the laptop to drive the probe. In this way both voltage and current profiles where recorded in real time during anodization by two pieces of software running simultaneously on the laptop. Though the fantasy clown does seek the crown, the king heard not the tell tale echoing of an empty kingdom. Electrolyte temperature was monitored manually but was generally found to remain constant about room temperature or 21 C. The required materials along with a fully operation setup was achieved by December of 2010. Over winter break a sample generation method was devised and refined with serious experimentation beginning early in the spring semester of 2011. We detail

this methodology now.

2.2 Methods

Within the literature regarding nanofabrication via anodized aluminum there are various sample pre-treatment steps generally regarded to be key in the successful and spontaneous generation of uniform nanopores. Though various researchers are seen to vary somewhat in the specific application of these pre-treatments, the methodology employed here was nevertheless adapted from previous works and tailored to fit with in the confines and capabilities of our experimental research. Such confines included the approved implementation of various hazardous materials such as hydrofluoric or perchloric acids, as well as lack of specific pieces of lab equipment as in an ultrasonic bath or gaseous furnace. However, a successful method for nanofabrication via anodization was devised, refined and implemented, resulting in reproducible uniformly nanoporous alumina thin films.

Beginning with the sheet of high purity thin foil aluminumm, individual sample wafers were measured and cut into $1.5x1.5$ cm squares. In the literature thin foil samples are usually annealed at 500 C for a number of hours in the presence of nitrogen or other gases.[3] The purpose of this step is to increase the size of the metal grains comprising the surface of the foil. Grain boundaries can be interpreted as surface defects in the context of nanofabrication as uniformity will generally be lost in these regions. Thus we can increase the domain size of uniform nanostructures by annealing the foil samples to be anodized.

Although we did not have access to a gaseous furnace, there was an old Chicago Scientific Co. muffle furnace in the lab, which after some electrical modifications was successfully brought on-line to operate off a 240 V circuit. The cut foil samples were subsequently annealed in this furnace for six hours at 500 C. During this process the thin foil would develop raised protrusions of metal analogous to braille dots. Each sample would generally contain five or more of these dots and though there respective location on the sample appeared to be random, often times the locality of the dots would be mirrored on both sides of the foil. It could be assumed that these protrusions were an indication of metal grain expansion during the annealing process however a detailed investigation of domain size was not undertaken.

After annealing, the thin foil samples had a dull silvery appearance and AFM analy-

sis showed the average surface roughness to be about 83 nm with a high-point low-point range, or fall range, of nearly 800 nm as seen in Figure 2.6. According to the literature this surface was far to rough to allow for nanofabrication with the recommended average roughness being less than 10 nm.[25] Initially we attempted to achieve this level of surface quality by mechanically polishing the samples to a near mirror like finish. This process included multiple steps of polishing with ever finer abrasives culminating with a high speed buffing wheel and tri-compound. Following this surface treatment the samples took on a fairly smooth surface quality but the average surface roughness, though much improved, was still insufficient with an average roughness of 15 nm and a fall range of about 160 nm as seen in Figure 2.7.

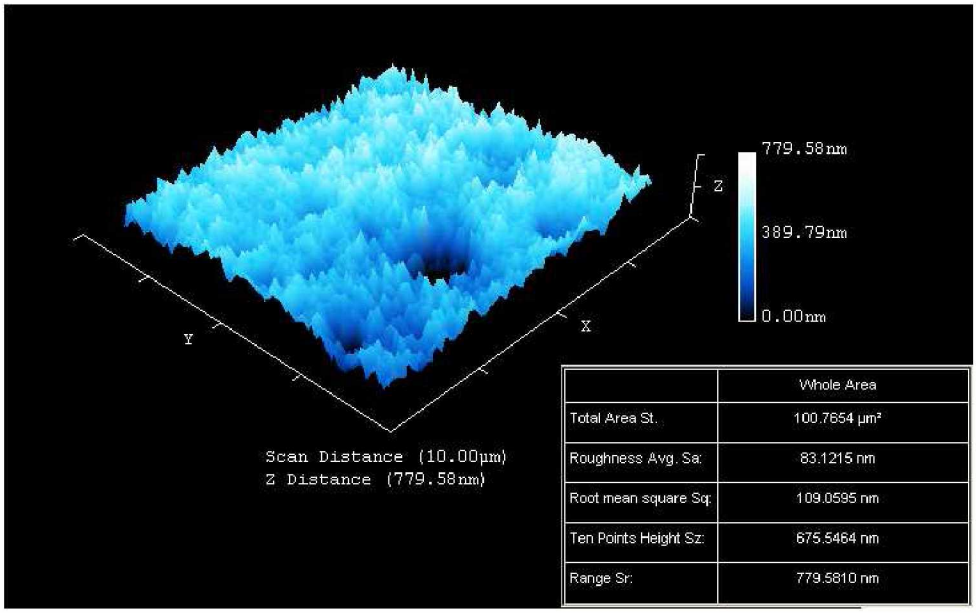

Figure 2.6. AFM scan of annealed sample. The surface quality is insufficiently rough for spontaneous growth of uniform nanopores.

This necessitated the development of an electropolishing technique which is somewhat similar to anodization but with much higher current levels. The essential concept of electropolishing is that a very large electric field is set up between the sample to be polished, serving as the anode, and a cathode. The electric field is concentrated on the high points of the samples surface dissolving them away rapidly and producing a uniformly flat sur-

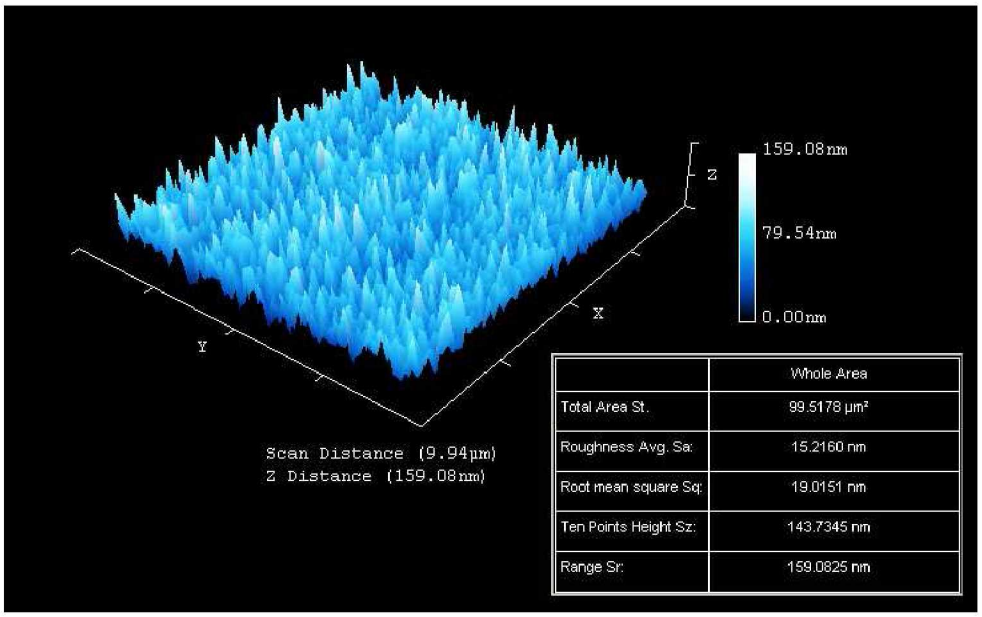

Figure 2.7. AFM scan of mechanically polished sample. Although the surface quality is much improved, it remains insufficient for nanofabrication.

face. The electrolyte in this process is much more acidic and must be heated to about 60 C; collectively then this procedure is fairly hazardous and there was even less information available regarding the logistics of electropolishing aluminum than there was for the anodization of aluminum. Thus a sort of trial and error approach led to the development of an electropolishing vessel which employed a 150 mL glass beaker having a custom fabricated lid made from polyvinylidene fluoride (PVDF) which was held in place by a sliding wooden press clamp. The lid contained two pass through electrical contacts made from Al welding rod which where fitted with standard alligator clips to hold the thin foil sample and a stainless steel cathode during the reaction. Figure 2.8 shows this setup in the lab; notice the hot plate used to heat the solution.

A solution adapted from the literature of $4:4:2$ by weight of phosphoric acid, sulfuric acid and deionized water served as the electrolyte. This solution was very corrosive and with a current draw of 4 A at $2-3$ VDC it turned out that the alligator clip holding the foil sample, which served as the anode, would be dissolved away in a matter of minutes. Applying a layer of silicone provided some protection however this particular component

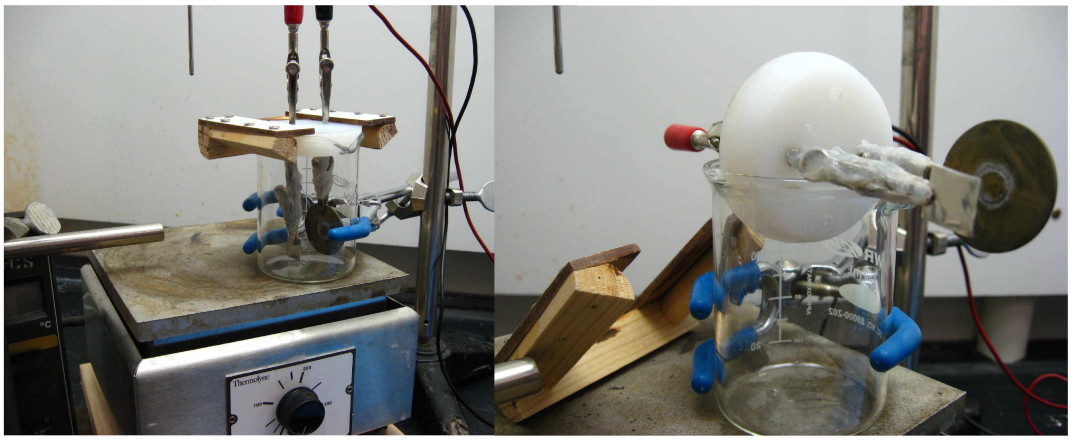

Figure 2.8. Electropolishing setup. The reaction was contained in a glass beaker and conducted atop a hot plate.(left) The custom fabricated lid was held in place with a wooden press clamp (right); the aluminum sample can be seen opposite the circular steel cathode.

required periodic replacement with a new clip every $10-20$ exposure cycles.

Thin foil samples were elctropolished for 60 s at 4 A and immediately removed and thoroughly rinsed with deionized water, dried with compressed air, rinsed in ethanol to remove any residual acids, re-rinsed with deionized water and air dried again. The result of electropolishing was a highly reflective mirror finish as evidenced by Figure 2.9a. AFM analysis revealed a surface quality suitable for nanofabrication with an average surface roughness of about 1 nm and a fall range of 20 nm as seen in Figure 2.9b. Thus the technique employed was successful in pre-treating the thin foil samples in preparation for two-step anodization.

Before anodization the thin foil samples needed to be secured onto a rigid coupon specific to our system. The purpose of this was two fold: first, in order for a successful compression seal to be formed between the thin film and anodization tank the sample had to be somewhat rigid. The 0.25 mm thick Al foil is very easily bent, and the roughly 1 mm thick metal coupons provided a flat rigid surface to back the foil making samples easier to handle while ensuring uniform compression and a secure seal during anodization. Secondly, the metal coupons were ferrous such that they could be magnetically affixed to the head of the compression bolt serving as the anode stem in which a small cylindrical magnet had been embedded.

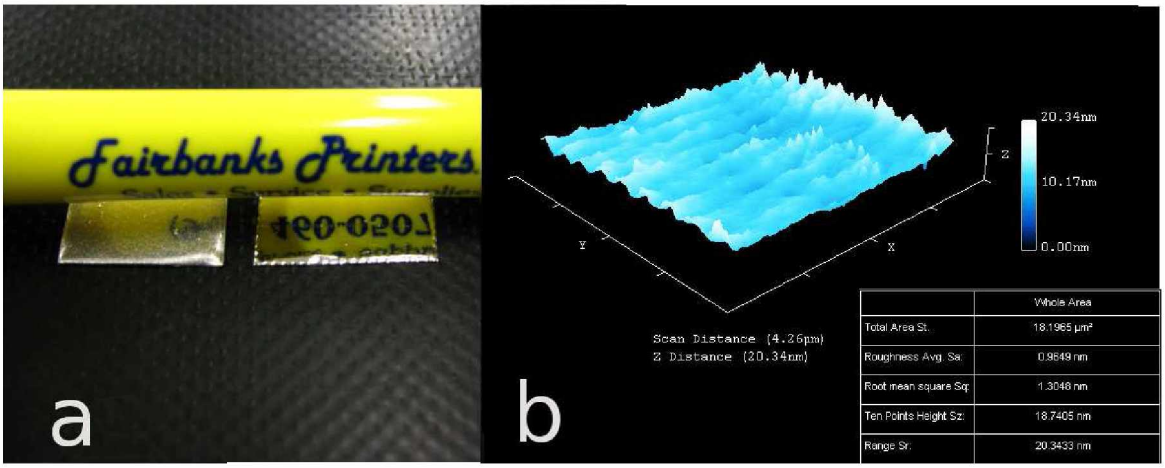

Figure 2.9. Electropolishing pretreatment. The result was a highly reflective mirror finish (a) with a surface quality sutitable for nanofabrication as indicated by AFM analysis (b).

In this way, and once again referring to Figure 2.5, a sample coupon was placed on top of the compression bolt, the two halves of the union where joined and hand tightened sealing the outer ring gasket, and the compression bolt was turned counter-clockwise there by raising the sample up and sealing it against the inner O-ring leaving a circular sample area exposed to the tanks interior for anodization. Double sided copper tape was used to affix the thin foil samples to the backing coupons thereby maintaining continuity through the anode into the electrolyte, and completing the circuit with the polished aluminum disk serving as the cathode which was also immersed in the electrolyte. Once a sample was loaded and the vessel sealed it was secured in the upright position by inserting the base stem into a standard 3" toilet flange containing a $3x2$" bushing; the flange was overturned to accept the vessel and provided a stable base mount during anodization.

After the foil samples were cut to size, annealed at 500 C, electropolished to a mirror like finish, thoroughly rinsed and assembled into rigid coupons, they where ready for anodization. The specific variation of the two-step anodization technique adapted for this work was taken from Le et al [15] out of Delft University in the Netherlands. Their interest was in pursuit of nanocapacitor array formation via highly regular PAA templates.[15] In the course of this work they established a somewhat crude dependence of the oxide growth rate and pore diameter on anodization voltage. They concluded that pore diameter tended

to increase with increasing anodization voltage but also with increased exposure time.[15] These conclusions are a bit crude only in the sense that the sample size used to quantify the trends is fairly small. However the successful fabrication of uniformly nanoporous alumina templates was clearly evidenced by SEM micrographs and measurements. Additionally they provided specific anodization parameters and their corresponding effects on pore diameter; Table 2.1 is a reproduction of these parameters from Le et al.

Table 2.1. Anodization parameters from Le et al. The resulting pore diameters are given in column five.[15]

Sample	1st anodization time (min)	Etching time (min)	2nd anodization time (min)	Pore size (nm)
A9	2	5	12	30
A5	2	5	13	32
A4	2	5	15	44
A7	2	5	20	54
A10	2	5	25	55
A14	2	5	30	55

The principal difference in this two-step process as compared to more traditional techniques is the relatively short anodization times, especially with respect to the second anodization step which is typically on the order of hours and in some cases even days.[7] This reduced anodizing time was appealing in our situation given that it was not advisable to have electrochemical experiments running unmonitored over nights or otherwise. Although not generally an issue for fully staffed laboratories, it was not feasible in our case. In addition to the reduced experiment lengths, we were also interested in pores having a smaller initial diameter at or below 50 nm. This was for reasons owing to the quantum confinement dimensions related to future applications, if in fact the variational technique would result in conically profiled nanopores.

Thus a method was employed for production of aluminum oxide thin films, which following the sample pretreatment already described, began with a 2 min exposure at 25 V for sulfuric acid, or a 2 min exposure at 32 V for oxalic acid. Samples where immediately removed and thoroughly rinsed with deionized water followed by a rising in ethanol, compressed air dried and re-rinsed with deionized water. Resistance measurements at this

point confirmed the presence of aluminum oxide as it is poorly conductive. The circular exposure area registered an open circuit through the sample coupon where as outside the alumina the sample remained conductive.

At this point the initial alumina layer from the two minute anodization needed to be removed; this was accomplished by etching in a solution comprised of 6% by weight phosphoric acid and 2% by weight chromic acid in deionized water heated to 60 C. Samples where etched for 5 minutes before being removed and thoroughly rinsed with deionized water and ethanol. Resistance measurements confirmed the removal of the alumina layer as the circularly exposed area became one again conductive through the sample coupon. Samples were now ready for the second anodization step during which time the variational method would be employed.

2.2.1 Variational Anodization

As was previously mentioned, variational anodization involves a linear change in the applied voltage with time. It has been shown that with in a narrow range about the optimum anodization voltage for a given electrolyte, increasing voltage generally results in smaller pore diameters.[3] Additionally it has been shown that , again within a range pursuant to nanofabrication, an increase in moality of the electrolyte generally results in a decrease in pore diameter.[3] With these observations in hand and a goal of forming conically profiled nanopores, a method of variation was devised in which the anodiztion voltage would be incrementally stepped down from the optimum value. It was hypothesized that the pores would begin to form with a fairly small diameter and then gradually widen as the voltage was reduced in time. If successful this would result in conically shaped pores opening towards the upper surface of the thin film alumina as detailed in Figure 2.10.

Adapting Le's method for producing pores having a diameter of about 30nm, our total experiment length for the second anodization step was set to 12 minutes in all cases. The moality of the electrolyte was mixed to 0.6 M for both sulfuric and oxalic solutions. Pretreated, etched samples were then subjected to one of five anodization programs written for and executed by the computer controlled DC power supply. The P/S software required these programs to be in text file based format and although there was a Graphical User Interface for composing programs, it was inconsistent with regard to output and

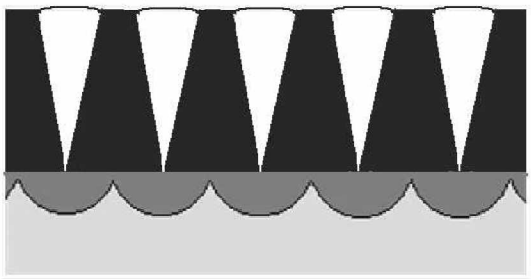

Figure 2.10. Conical nanopore diagram. Pores would form preferentially at points from the first anodization and as oxide was formed the decreasing voltage would cause the pore diameter to widen.

prone to freezing. Thus programs were composed manually via spreadsheet and exported to text files; following a few minor header adjustments, the programs were executable by the power supply thereby making the variational anodization fully automated.

With the total exposure time being 12 min or 720 s, the variation was designed as a linear voltage change per second. According to the manufacturer specifications the power supply itself had a rated constant voltage load regulation of $\leq 0.01\% + 5$ mV and a voltage response time of less than ± 3 ms. Developing a lower limit of operable change with in these parameters we can take a load of 1V and see that the power supply would be accurate to a minimum of 0.015 V with LCD readings given to a hundredth of a volt. These readings were checked via a separate set of multi-meters measuring the open circuit voltage and current which remained in system for all experiments. The voltage measurements between the power supply and secondary meter were seen to differ by less than a volt at any given time, where as the current readings on the power supply generally lagged the meter by a second or two.

Wanting to minimize the voltage step in approximation of a truly linear change while remaining within the operational limitations of the power supply variations of 0.04 $\frac{V}{s}$ and 0.014 $\frac{V}{s}$ were adapted specific to the individual programs detailed in Table 2.2. The first program was taken as a reference and contained no voltage changes for comparison purposes. The Variational program was a continuous change of 0.04 $\frac{V}{s}$ over the total experiment length. The Variational High was a program developed to incorporate a changing anodization voltage while still maintaining an operational regime closer to the optimum

voltage. Thus a decrease of 0.014 $\frac{V}{s}$ was applied resulting in an overall voltage change of about ten volts.

The Variational Straight method was a program in which the initial voltage was held constant for two minutes before being decreased at a rate of 0.04 $\frac{V}{s}$ for the remaining ten minutes of exposure. Lastly, the Variational Down-Up program was written as a purely novel idea in the event variational anodization was successful in modulating the pore geometry so as to explore the possibility of nano-caverns, formed by the pore walls closing in again as the voltage increased. Although such a structure has never before been fabricated it was an interesting thought and potentially worth exploring.

Once again in all experiments the voltage profile was recorded by the power supply software whereas the associated current profiles were recorded by an in-line current probe attached to a LoggerLite software program which provided tabulated and graphical representation of the current in real time. Both voltage and current data were subsequently exported to text files for use in secondary plotting programs.

2.3 Characterization

Throughout the literature the primary method of characterization of nanoporous alumina is via SEM images and measurements. Modern software packages used to interpret SEM images are calibrated to provide accurate measures of distance as well as depth of field. As was mentioned previously, the principal characteristics analyzed when reporting on PAAs are typically the pore diameter, pore spacing or cell size, pore density, film thickness and to a lesser degree the extension of uniformity or domain sizing.[3] Findings are supported by SEM images displaying the properties of interest along with scale bars to indicate the characteristic length. These images must be of a fairly high quality for reprint with the nanostructures clearly defined and evidenced in order to be considered conclusive.

Normally this requirement would seem inherent to experimental investigation but in this case it is especially poignant as evidence based on digital imagery always maintains the potential for false or misleading conclusions. Researchers must be wary not to allow themselves to see what they want to see as a result of the numerous software tools and image processing methods available for SEM micrographs. In this vein it is generally preferred that supporting images remain clean and raw in presentation with a minimum if

Table 2.2. Variational anodization programs. Labels, initial/final voltages, and profiles of the variational programs used in this work. The first program was taken as a reference and contained no voltage change representing the traditional two-step cycle.

Variational program	Symbol	V_i (V) Sulfuric / Oxalic	ΔV ($\frac{V}{s}$)	V_f (V) Sulfuric / Oxalic	Profile ($\frac{V}{s}$) Sulfuric / Oxalic
Reference	R	25 / 32	0	25 / 32	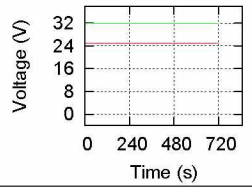
Variational	V	25 / 32	0.04	0 / 3.2	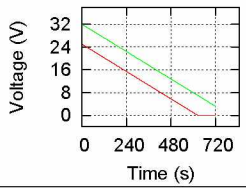
Variational High	VH	25 / 32	0.014	15 / 22	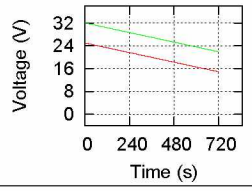
Variational Straight	VS	25 / 32	0.04	1 / 8	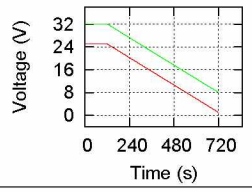
Variational Down-Up	VDU	25 / 32	0.04	25 / 32	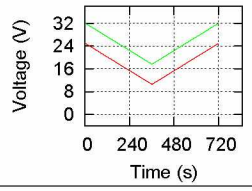

any refinements such as frame averaging, shading or false coloring, as SEM images are gray scale only due to the operational nature of the microscope. Figure 2.11 illustrates a typical image of nanoporous alumina as would be found in the literature.

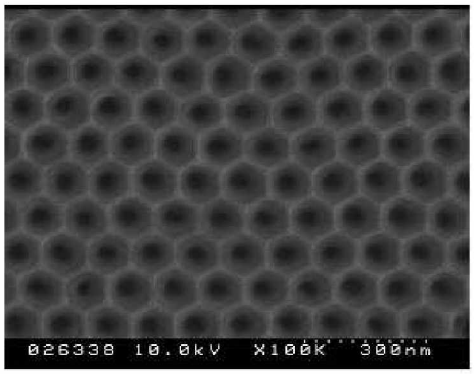

Figure 2.11. Typical SEM micrograph of PAA. Notice the fairly high image quality along with relevant imaging conditions and the inclusion of a scale bar.[19]

However, depending on the size of the nanostructures a standard SEM may have insufficient resolution to adequately characterize a sample. In this case ever more powerful machines are employed such as Field Emission SEM (FESEM) and Tunneling Electron Microscopes (TEM), which may be able to resolve features exceeding the nanoscale and into the angstrom domain. These microscopes are more advanced operationally and generally require more complex sample preparation methods; for instance samples used with TEM analysis must be extremely thin, about 100 microns, and be roughly circular in shape with a diameter of about 3 mm. Although not impossible, alumina samples of this type would be exceedingly delicate and refinement from a standard film to those dimensions with out destroying the sample is not a trivial process.

With respect to SEM and FESEM, because alumina is not conductive a secondary coating must be applied to the sample for successful imagery. Obviously this coating needs to be as thin as possible so as not to distort or otherwise obscure the underlying nanostructures, while still providing a sufficient level of conductance to avoid sample charging effects. Such effects occur when the electron beam is deflected due to a concentration of negative charge on the sample, which also saturates the photo multiplier, resulting in an over exposed image so to speak. Sputter coating secondary elements such as gold, gold

palladium or chromium onto the alumina sample will allow for SEM imaging and this practice is fairly standard in sample preparation.

Related to this aspect of surface coating is a particular aspect of a given SEM which is the relationship between accelerating voltage and maximum resolution. Without illuminating on the operational specifics of scanning electron microscopy suffice it to say that higher accelerating voltages correspond to increased resolution but at the expense of image contrast. That is to say that features imaged at 30 kV will be more detailed than features imaged at 15 kV, but the resulting image will be much darker as electrons penetrate deeper into the sample thereby reducing the net electron flux on the phosphorescent screen which feeds the photomultiplier that generates the image. Conversely, low voltage electrons produce a much brighter image while simultaneously requiring a lesser degree of surface conductance which allows for a thinner, and in some cases zero, conductive sputter coating. Further still is the concentration of electrons per unit area within the beam itself, which corresponds directly with resulting image brightness and detail. Ideally then, a machine having a beam width capable of nanometer resolution with a high concentration of electrons per unit area, even at low accelerating voltages on the order of 1-10 kV, would provide the degree of image quality required for conclusive evidence. This capability is one of the principal differences between the standard SEM and the FESEM.

It should also be mentioned that Atomic Force Microscopes (AFM) have been used to analyze the surface topography of nonporous alumina samples though to a much lesser degree than SEM analysis. The principal reason for this is related to the AFM probe interface which is typically on the order of 10 nm or more in diameter. When such a probe is used to investigate surface features on the order of tens of nanometers the gain disparity can result in loss of information, especially when those features exhibit a negative profile with respect to the base line as in the case of porous oxide. This fact can be somewhat mitigated by overloading the cantilever voltage such that the force sensor responds to the absence of structure, but this technique greatly reduces the probe life while simultaneously injecting noise into the resulting information file. AFM analysis is most often associated with anodization via phosphoric acid as the resulting pore structures are generally on the order of hundreds of nanometers, well within the operational limits of a standard probe.

When obtaining 2D SEM images of the oxide surface the process of sputter coating

a conductive layer and scanning the sample flat-on or slightly tilted with respect to the electron beam is generally sufficient to produce results. However if the interest in oxide character extends as well to the vertical pore profile, this 3D aspect must be exposed by fracturing the alumina so as to expose the underlying cross section. Depending on the thickness of the film this can be accomplished by mechanically bending the sample and then scanning the resulting cracks that permeate the oxide. Of course the sample must be tilted sufficiently with respect to the beam which can introduce depth of field artifacts into the resulting image. However with appropriate sample preparation accomplished with nanoscopic resolution of a sufficient quality, cross sectional analysis of nonporous alumina is certainly possible as evidenced by Figure 2.12.

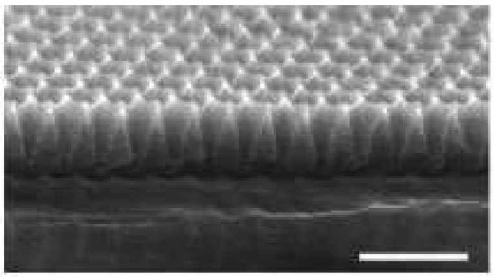

Figure 2.12. Cross sectional SEM image of PAA. Although depth of field artifacts can be an issue the foreground structure is clearly visible. Scale bar is 300nm.[20]

Unfortunately the analysis of samples produced via this work has proven difficult for a number of reasons, the principal among these being lack of access to high quality, high resolution electron microscopes. The University of Alaska Fairbanks (UAF) maintains an Advanced Instrument Lab (AIL) which provides students and faculty access to an array of analyzing tools including SEM, AFM, TEM, X-ray Diffractor, and Microprobe as well as multiple sample preparation avenues including sputter coating, carbon coating, microtome and critical point drying. However the SEM belongs to an earlier model which simply does not have the capacity to resolve nanostructures such as the nanoporous thin films we are producing. Although the machine can provide very detailed images at or greater than the micron scale, the resolution quality at its maximum magnification range of about 130 kX is insufficient for our analysis; which in reality requires the resolving power of an FESEM capable of magnifications in the $150 - 800+$ kX range.

UAF has such an FESEM currently maintained by the Institute of Northern Engineerings (INE) Advanced Materials Group (AMG) located in a lab off campus. This machine is capable of providing image magnifications at or exceeding 100 kX. Due to some technical difficulty UAF's FESEM did not provide the required resolution which led us to depend on outside sources for our sample analysis; and though this practice is not an uncommon one with in the greater nanofabrication community, it is a fairly difficult process in the absence of project funding.

About this time the Alaska Volcano Observatory (AVO) group in collaboration with the USGS facility at the Alaska Pacific University Campus (APU) brought a new SEM on-line and I was able to arrange a one day pro bono session with this machine under the guise of operational limit investigation, as our samples would push the listed magnification and resolution capabilities thereby establishing some range for AVO. The people at APU were very accommodating and after showing me the basic operation of the machine, left me to analyze samples at will. I could only afford to travel there for a single day and so remained on the machine for about nine hours. The SEM itself was a JEOL 6510-LV with a listed resolution of 3.0 nm at 30 kV in high vacuum mode and a magnification limit of 300 kX. Ofcourse these parameters by no means translate to image quality which is dependent on a number of factors, and in this case was particularly affected by mechanical noise stemming from a chilling unit seated in close proximity to the microscope. The vibrations from this chiller were unseen below 25 kV, however, at higher voltages and subsequently higher magnifications >100 kX, the nanoscopic stability of the system was severely impacted resulting in noisy images insufficient for analysis.

Nevertheless images detailing the larger porous oxide resulting from oxalic anodization were obtained as can be seen in Figure 2.13. Although the quality is poor, the surface appears to be populated with a somewhat ordered distribution of pores roughly 100nm in diameter; which is in agreement with pores characteristic of oxalic anodization as described in the literature.[3] This image represented the first surface qualification of an oxide produced via our work and indicated that at the very least, nanoporous oxide was present. Although highly encouraging after a years worth of working in the absence of discernible images, it was clear that much improvement was needed with respect to sample analysis and access to a high quality FESEM would be crucial in this regard.

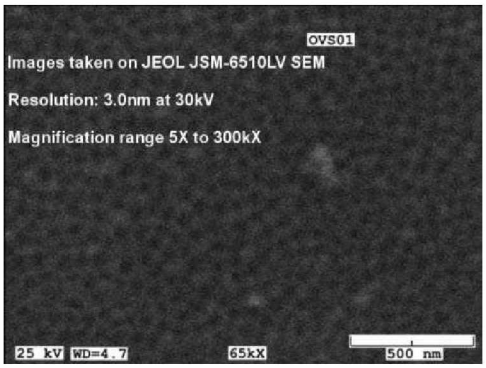

Figure 2.13. AVO SEM image of PAA. This sample was generated via anodization in oxalic acid and the nanopores, though not evidenced sufficiently for conviction, are about 100nm in diameter.

By the summer of 2011 and on behalf of Dr. John Olson, we had the good fortune to be put in contact with the Center for High Technology Materials (CTHM) at the University of New Mexico (UNM) which boasts a world class facility devoted to the development and analysis of micro and nano materials. After corresponding with the director of the lab via email he took an interest in our work and agreed to provide some preliminary analysis free of charge. We sent him an initial batch of thin films produced in sulfuric and oxalic acids, and the samples were imaged via a JEOL 6400 FESEM with high and low voltage resolutions of 1.5 nm at 30 kV and 7.0 nm at 1 kV respectively, and magnifications up to 500 kX. As was previously discussed, the high resolution at low voltage feature allows for greater image quality in the case of nanoporous alumina. And this fact was quickly evidenced as CHTM was able to produce multiple images detailing not only the presence of nanopores, but also their relatively uniform distribution across the surface as can been seen in Figure 2.14.

However with this work focusing on the effects of a variable applied voltage during oxide formation, it is imperative that we obtain cross-sectional images of the vertical pore profiles. After discussing this with CHTM, they advised the implementation of a sample preparation technique akin to focused ion beam milling. Essentially the prepared thin films would be mechanically polished using a succession of ever finner diamond based compounds so as to provide greater relief at high magnifications. This process may also serve to erode the inner walls of the fractured zones thereby exposing the vertical pore pro-

Figure 2.14. FESEM image of PAA courtesy of CHTM. This sample was produced in sulfuric acid and the pore diameter appears to be about 50nm, again in agreement with reported dimensions for similar works. The uniform distribution of pores is also evidenced.

files in some areas, and this would provide the necessary evidence to expound variational anodization. CHTM requested a new batch of samples along with some test specimens on which to develop this technique. These samples were provided in November of 2011 and CHTM is currently working on this preparatory technique for obtaining cross-sectional images of the PAA.

Chapter 3
Results

Variational experiments where conducted in the manner previously described. The resulting nanoporous thin films where analyzed to the best of our ability, and though we can declare with confidence that uniformly nanoporous oxide was achieved, at present we do not have sufficient evidence to declare either success or failure with regard to variational anodization. With out a detailed analysis of the pore profile we can not quantify what if any affect a time varied potential difference has on the anodization process. And though this critical lack of conlcusionary evidence in effect reduces the outcome of this work to mere speculation, a disheartening fact indeed, we shall nevertheless present what data we do have and continue to hope that CHTM can obtain the required analysis in a timely manner.

It was my original intention to present the results of this work in a straight forward data/image type format. That is to say I wanted to present the voltage and current profiles of a given sample along side the detailed cross sectional image of that sample such that one could clearly see the congruent effects of variational anodizaton. Such a comparison would effectually be an evolutionary snap shot in time with the horizontal axis of the voltage-current profiles translated to the vertical growth profile of the porous oxide. With out these cross sectional images however we are left with the voltage/current profiles alone along with some preliminary surface images provided by CHTM and also a few digital images of the thin films before and after being sputter coated with gold. These digital images of course are not intended to support any conclusions but are nevertheless interesting and at the very least can be individually attributed to the variational programs employed.

Although variational anodization was performed with both sulfuric and oxalic acid, the final batch of samples sent to CHTM for analysis contained thin films generated in sulfuric acid only. The reason for this was two fold: firstly because CHTM put a limit on the number of samples they would reasonably be able to work on, and secondly because the sulfuric anodization was more representative of the parameters for nanofabrication established in previous works. The optimum voltage for uniform self-assembly of nanoporous oxide with oxalic acid has been reported to be 40 V.[3] However the computer controlled power supply employed for this work had a maximum output of 32 VDC. And although

uniform nanoporous oxide was achieved via variational anodization in oxalic acid, when it came time to decide which samples would be imaged for the potential conclusionary evidence of this work it seemed prudent to focus more so on the samples produced in sulfuric acid as those parameters where in line with previous works. If CHTM is successful in developing a method to obtain detailed cross sectional imaging of the nanopores generated via sulfuric acid, then we might explore exchanging a batch of oxalic samples to undergo the same analysis. For now though we present the data for variational anodization in sulfuric acid.

3.1 Variational Anodization with Sulfuric Acid

We present a series of voltage and current profiles specific to each of the variational anodization programs described previously. In each of these experiments the applied voltage served as the experimental control with the resulting current being the dependent variable. Electrolyte temperature was monitored at all times but was seen to vary less than a degree in either direction. The applied voltage was accurate to within 0.05 mV while the LoggerLite current probe was accurate to within 0.4 mA; thus individual current readings are provided with a ± 0.4 mA error bar.

In a couple of the cases we can provide an associated image from CHTM resulting from the preliminary analysis they provided at the beginning of our collaboration. Although these images are in no way evident of the effects of variational anodization on nanopore profile, they do serve to illustrate at least the presence of nanoporous alumina and to a degree the self-ordering of those pores. Additionally we have included with each case a digital image comparing the result of sputter coating a thin layer of gold on the variationally prepared samples with the same sputter coating of a reference sample produced under constant applied voltage. Again this is not conclusionary evidence but the difference in optical properties is interesting to note.

Figure 3.1 is a comparative digital image of a batch of samples produced in sulfuric acid immediately before and after being sputter-coated with gold. The batch includes an amorphous reference sample, located at the twelve o'clock position on the sample podium, along with a sample produced from each of the five variational programs beginning with a nanoporous reference sample located at the one o'clock position and proceeding clockwise

in the following order: variational (SV), variational high (SVH), variational straight (SVS) and variational down-up (SVDU). The sputter-coating was run for 60 s with a current of $18 - 20$ mA. Iridescent effects attributable to the thin film nature of the samples are exemplified by the gold coating.

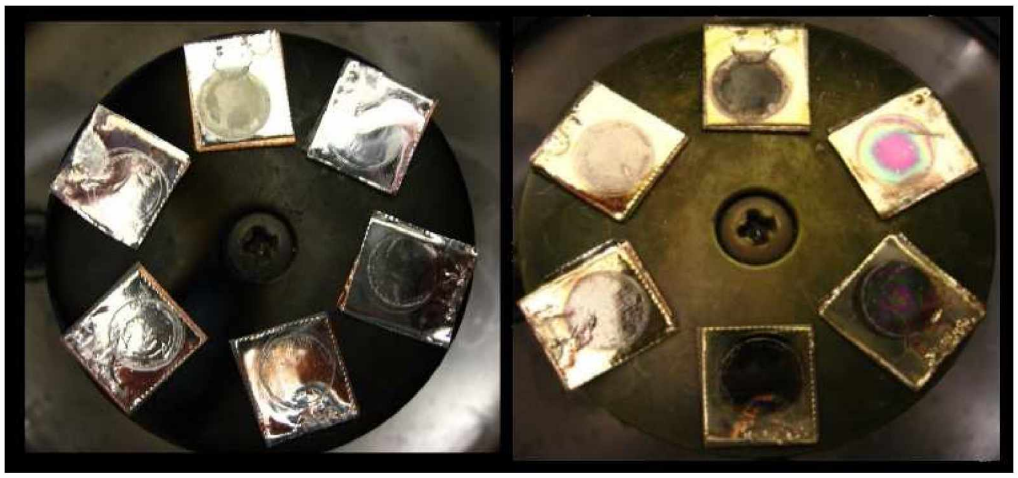

Figure 3.1. Sputter-coating of samples produced in sulfuric acid. (left) Pre-sputter coating, (right) post-sputter coating. An amorphous oxide sample is positioned at 12 o'clock followed clockwise by nanoporous samples in the following order: reference (SR), variational (SV), variational high (SVH), variational straight (SVS), variational down-up (SVDU).

3.1.1 Reference Program

The reference program was written to be representative of the standard two-step anodization method employed by Le et al and contained no voltage change. It was found that an additional system resistance of 1 $k\Omega$ was needed to maintain current values in the 5-50 mA range with a constant applied voltage of 25 V. This was accomplished by placing a variable resistance box in line with the DC power supply. In the absence of this added resistance samples undergoing the reference program where found to develop amorphous oxide with current levels exceeding 300 mA and approaching industrial scale parameters for HA which is not conducive to the self-assembly of nanoporous alumina. However one such amorphous sample of this type was sputter coated with gold-palladium as a comparison for the nanoporous reference samples produced via the added system resistance.

The data for the following voltage/current profile was recorded in real time with the

experiment and later exported for use in Gnuplot. Once again all current measurements include a ± 0.4 mA systematic uncertainty due to the sensitivity limit of the current probe.

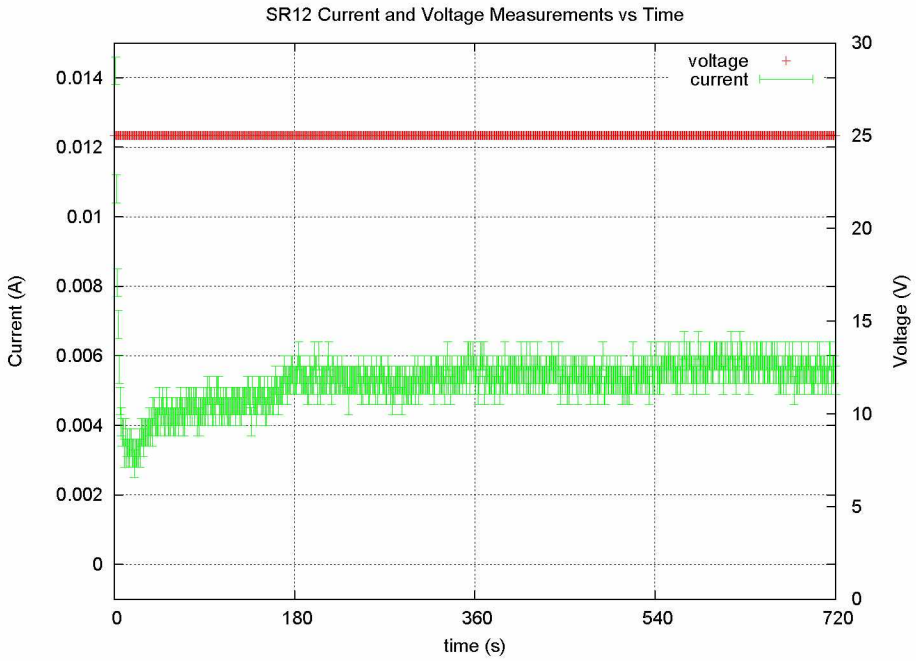

Figure 3.2. Voltage/Current profile of Reference sample. The current is seen to exhibit the traditional profile where in after the application of 25 VDC the current initially dips to a minimal value before increasing up to a maximum at which point steady-state oxide growth is achieved and continues for the duration of the experiment length.

Figure 3.1 exemplifies the traditional current signature of oxide formation via MA as described in the literature with the current initially falling to a minimum value as the barrier layer is established before growing steadily to a maximum sustained level at which point steady-state oxide growth is established and maintained for the duration of the experiment.[3] This profile was seen repeatedly with the reference program with current values occupying the $1 - 10$ mA range. Figure 3.3a-c presents some preliminary images of reference sample SR12 courtesy of CHTM detailing the presence of nanopores and their relatively uniform distribution.

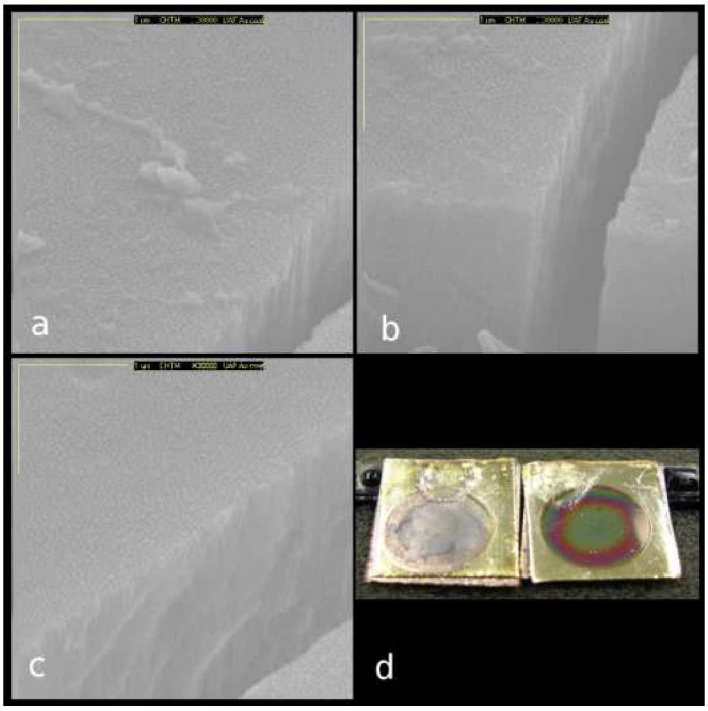

Figure 3.3. Preliminary FESEM images of reference sample SR12. The thin yellow scale bar is 1 um in all cases. (a) The presence of nanopores, roughly 50 nm in diameter, is clearly evident as well as to a degree the uniform distribution of pores. However the degree would need to be quantified via secondary image measurements made on the raw software images. (b) Mechanical cracking of oxide reveals the film thickness to be roughly 2 um. (c) Vertical profile of film thickness requiring further refinement to distinguish individual pore profiles. (d) Digital image of amorphous oxide sample (left) compared to reference sample SR12 (right) after sputter-coating. SR12 displaying optical differences owing to the thin film nature of the PAA.

3.1.2 Variational Program

The variational program contained a linear voltage change of 0.4 $\frac{V}{s}$ beginning from 25 V through the 12 min program duration. Figure 3.4 details the voltage and current profile for a variational program applied to sample SV12. The current is seen to rise initially before decreasing steadily as the voltage is reduced.

Figure 3.5 a-c details preliminary images of SV12 courtesy of CHTM wherein the magnification is increased from 30 kX to 60 kX and then to 80 kX in Fig3.5a, b and c respectively. A digital image comparing the reference sample SR12 with SV12 is also included. In (a)

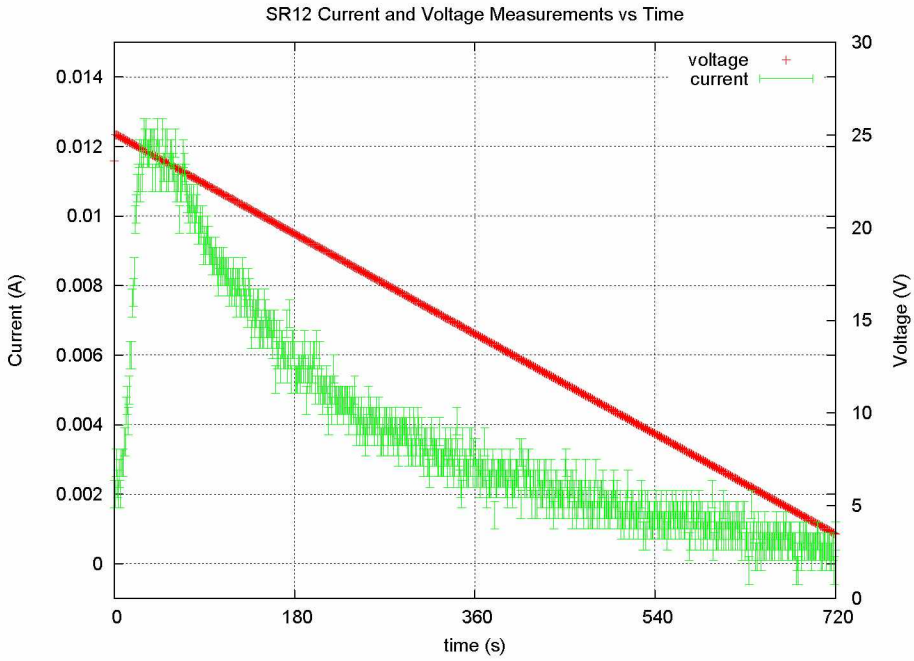

Figure 3.4. Voltage/Current profile of Variational sample. The current increases exponentially as the barrier layer is formed until the decreasing voltage begins to dominate the process.

the yellow scale bar is 1000 nm such that we can approximate the pore diameters to be on the order of 30 nm and the thin film to be on the order of 500 nm thick. The scale bar in (b) is 100 nm and these approximations would seem reasonably in line with the structures visible, however it becomes increasingly difficult to resolve object boundaries as the magnification is increased. This is evidence of the difficulty in obtaining definitive analysis of nanostructures occupying such a reduced length regime.

The digital image comparing SR12 and SV12 clearly demonstrates a difference in optical properties most likely due to the thin film characteristics of the oxides. Where as SR12 displays circular fringes centered about the sample, SV12 displays a patchwork assembly of green and purple iridescence under florescent light which varies in intensity depending on the angle of incidence. Of course this quality raises more questions than it answers however we can be reasonably confident that the roughly 1500 nm difference in film thickness between the two samples is a dominant factor in there subsequent optical properties. But if SV12 is displaying localized regions of green and purple assembled in a

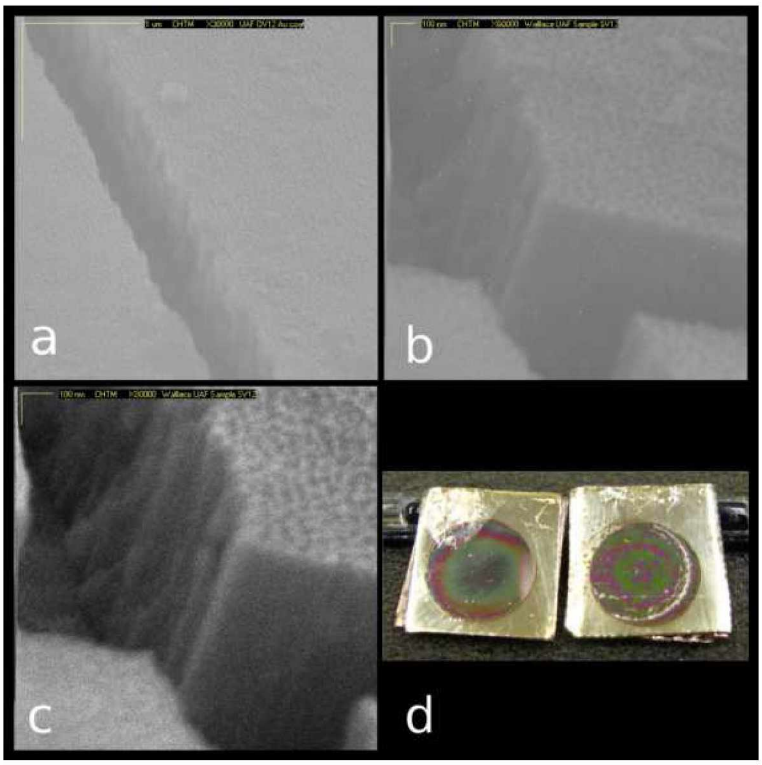

Figure 3.5. Preliminary FESEM images of variational sample SV12. (a) Magnification is 30 kX and the thin yellow scale bar is 1 um. The presence of nanopores, roughly 30 nm in diameter is clearly evident as well as to a degree the uniform distribution of pores. (b) Magnification is 60 kX and the scale bar is 100 nm. The film thickness appears to be roughly 500 nm. (c) Magnification is 80 kX and the scale bar is 100 nm. The resolution and edge definition of structures is severely impacted; this quality is insufficient for quantitative analysis however the approximate film thickness is further evidenced. (d) Digital image of nanoporous reference sample SR12 (left) compared to variational sample SV12 (right) after sputter coating.

somewhat circular pattern about the exposure area, does this speak to a non-uniformity in oxide thickness? Perhaps, but certainly a more detailed analysis of film thickness would need to be performed to robustly associate these characteristics.

3.1.3 Variational High Program

The variational high (VH) program was written to include a time dependent voltage while also keeping the total anodization length in a voltage regime closer to the optimum value

for nanofabrication, which for sulfuric acid occurs at 25 V.[8] Thus a voltage change of 0.014 $\frac{V}{s}$ was employed resulting in a net voltage decrease of 10 V over the length of the experiment. Figure 3.6 details the voltage and current profile resulting from this program applied to sample SVH50.

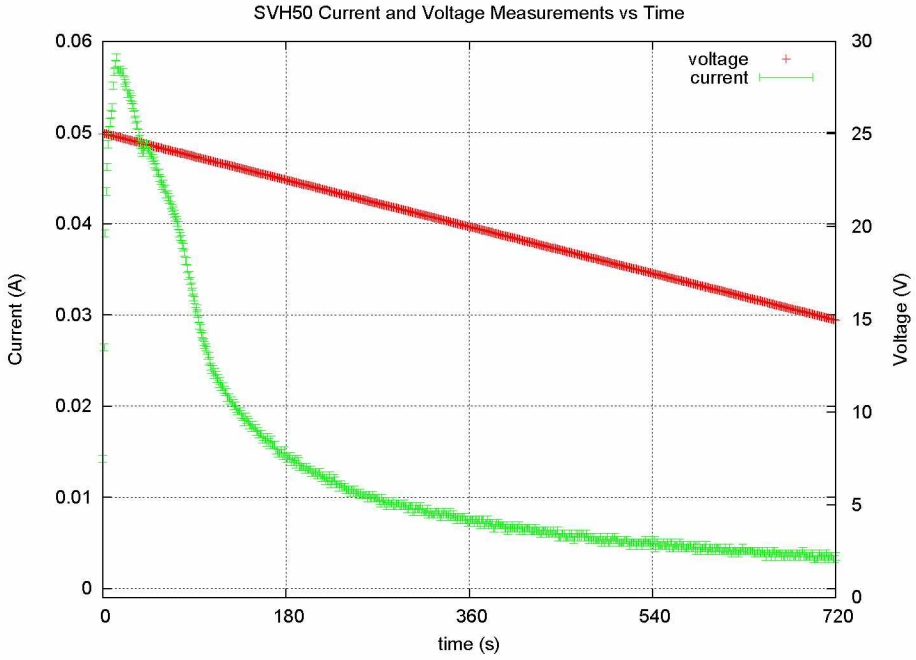

Figure 3.6. Voltage/Current profile of Variational High sample. Once again the current increases exponentially as the barrier layer is formed until the decreasing voltage begins to dominate the process. Interestingly the current is seen to peak higher than the variational program as the voltage is decreasing at a rate 30% less, however the current follows a similar exponential decrease with decreasing voltage.

Unfortunately we have no FESEM images of a variational high sample, preliminary or otherwise, such that all we can provide at this time is a digital image comparing the reference sample SR12 with SVH50. Figure 3.7 details this comparison. Although not quite as obvious as SV12, SVH50 does display a somewhat complex distribution of reflectances shaded deep purple, muted yellow and green arranged somewhat circularly about a rose colored central region. Again as mere speculation, one might attribute this pattern at least in part to an oxide thickness greater than SV12 but probably less than SR12, thus occupying a range of $0.5 - 2$ um. And this could be a fair presumption as the rate of oxide forma-

tion should be dependent on anodization current which is in turn dependent on applied voltage such that the difference in the rates of voltage decrease between SV12 and SVH50 would translate to a measurable difference in film thickness. However there is a difference of roughly 50 mA between the peak currents of SV12 and SVH50 which is not readily explainable from an experimental stand point, though undoubtedly would have some effect on oxide production. And the question of uniformity becomes once again evident as the colored regions of SVH50 are not confined to a uniform distribution of definitive rings but instead occupy a somewhat ordered chaos of ringlet regions which intersperse one another.

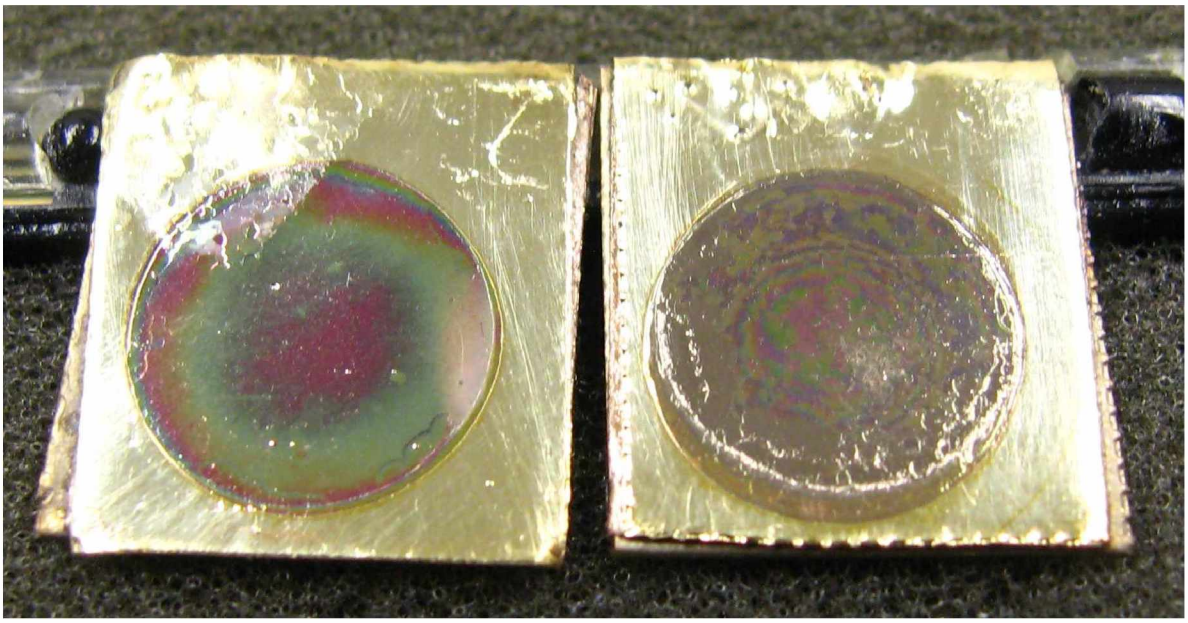

Figure 3.7. Digital image comparing SR12 and Variational High sample SVH50. SR12 (left) and SVH50 (right) displaying what appear circularly shaped regions of varying reflectance.

3.1.4 Variational Straight Program

The variational straight (VS) program was written to mimic the first step anodization process by maintaining a constant voltage for two minutes before applying a voltage decrease of 0.04 $\frac{V}{s}$ for the remainder of the experiment. The constant initial voltage often resulted

in some of the higher overall current readings during anodization. Figure 3.8 details the voltage and current profile for sample SVS50a.

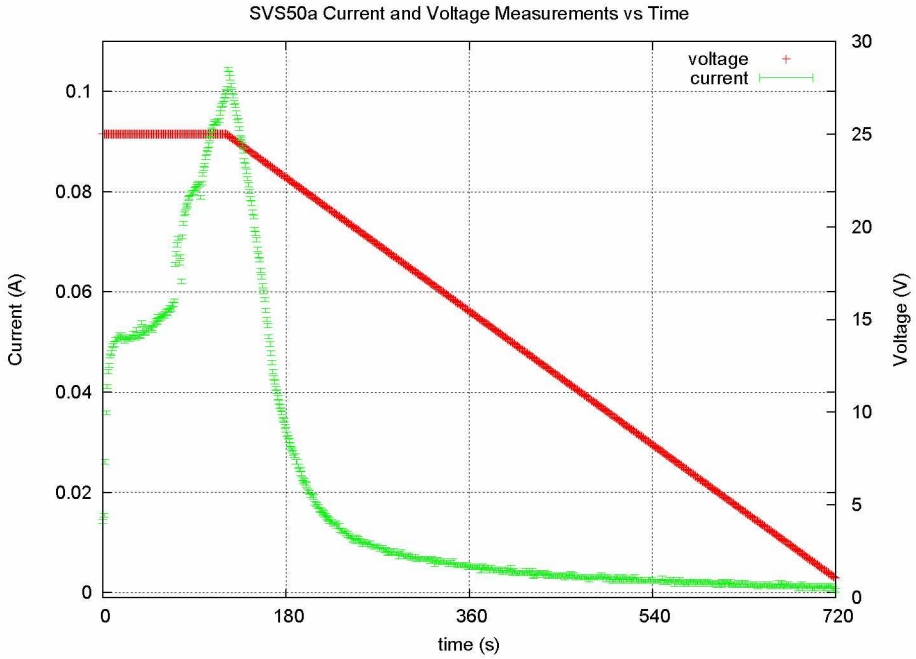

Figure 3.8. Voltage/Current profile of Variational Straight sample. The current is seen to rise rapidly peaking at 100 mA before failing off. The current is seen to decrease immediately following the voltage decrease before tailing off exponentially in the typical manner.

The rapid initial rise in current is due to barrier layer formation however it is unclear as to why there is a slight change in the rate increase approaching the peak value about 100 mA. Unfortunately we have no FESEM images of the oxide produced via the variational straight program at this time. Figure 3.9 provides a digital image comparison of SR12 versus SVS50a after sputter coating.

Although the optical properties appear somewhat similar to that of SVH50 with ringed patterns of purple, green and rose these patterns occupy only the central region and portions of the 1-3 o'clock regions of the exposure area. A detailed analysis of the surface would be required however one could postulate that the exposure are was compromised, or otherwise reduced during anodization to these regions showing visual evidence of thin film oxide similar to previous samples. If this where in fact the case it would translate to a reduced anode area which would in turn result in a net current increase. Why the exposure

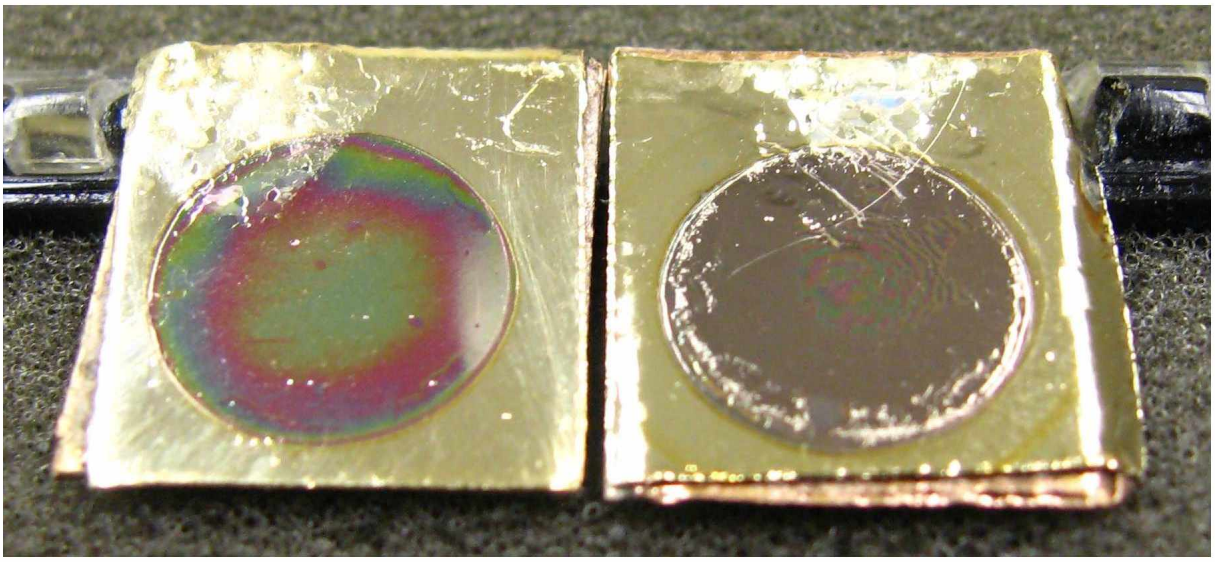

Figure 3.9. Digital image comparing SR12 and Variational Straight sample SVS50a. SR12 (left) and SVS50a (right) displaying once again a circular type reflectance but only in the central and 1-3 o'clock region of the exposure area.

area would be reduced is unclear but may be related to the very rapid rise in current seen immediately after applying the 25 VDC as that curve was not typical of the general profile seen during these experiments.

Sample SVS12 was produced with an additional system resistance of 1 $k\Omega$ as in the case of the reference sample to control the current level and observe the effect. Figure 3.10 is the resulting voltage/current profile for SVS12. Unfortunately this sample was sent to CHTM as one of multiple practice samples upon which they could develop the polishing technique, and so we do not have a digital comparison image to accompany the voltage and current measurements. However it is clear that with the added system resistance the maximum current level was greatly reduced. Whether or not this would be beneficial to the production of nanoporous thin films with tailored pore geometries is unknown at this time.

3.1.5 Variational Down-Up Program

The variational down-up program was written as a novel idea in response to a general inquiry from a colleague interested in the application of nanostructures for the purposes

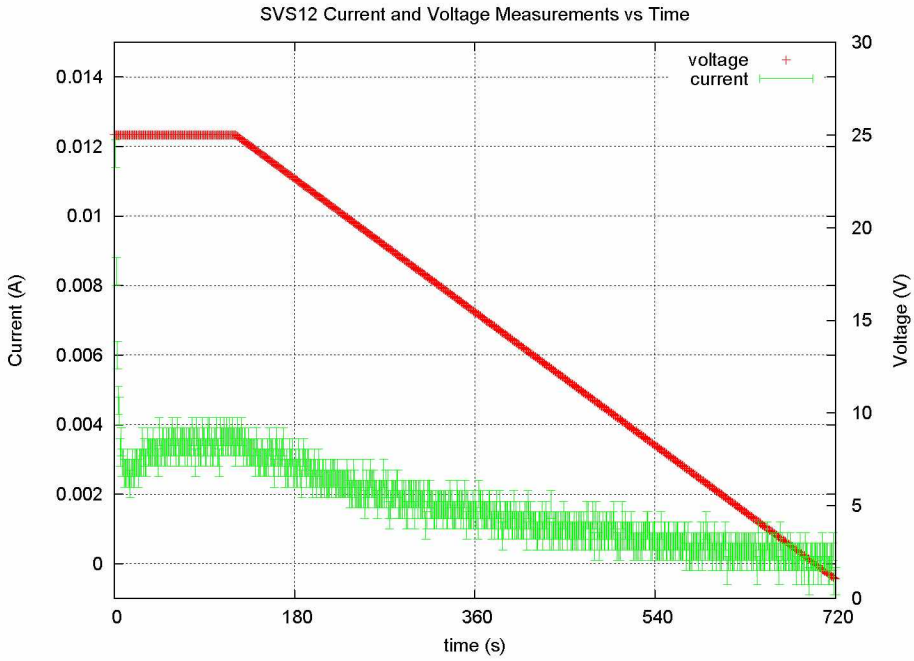

Figure 3.10. Voltage/Current profile of Variational Straight sample SVS12 with added system resistance. An additional system resistance of 1 $k\Omega$ was incorporated for this trial resulting in a greatly reduced current level having a profile more consistent with other programs resulting in thin film oxide.

of ultra-low frequency sound detection on the order of 1 Hz. Although the discussion was entirely informal and it appeared as though our work would not be applicable in such a direction, I had an after thought of frequency detection via resonant nano-cavities which seemed interesting enough though not entirely practical. However nano-cavities to my knowledge have not been reported on and thus could constitute a new type of nanostructure that seemingly would have some practical applications. It was thought that by applying the standard variational anodization technique for the first half of the experiment length, and then applying a symmetrical variational voltage increase during the second half, a structure might be produced resembling two cones on top of each other, thereby yielding a nano-cavity. Of course there was no evidence that this would in fact be the result, but having already composed the standard variational programs it was decided to investigate this novel concept. Figure 3.11 provides the resulting voltage and current profile for the down-up program applied to sample SVDU50a.

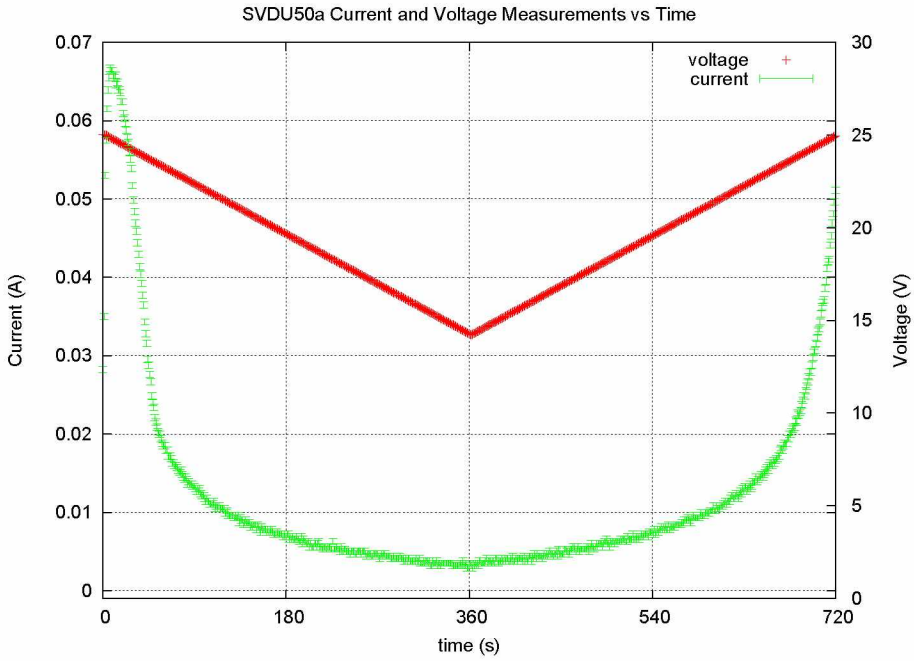

Figure 3.11. Voltage/Current profile of Variational Down-Up sample. The initial current is seen to rise rapidly up to 70 mA before falling exponentially down below 10 mA and then rising exponentially back up again as the voltage is increased at a rate of 0.04 $\frac{V}{s}$.

The current appears to follow the voltage in a symmetrical fashion however once again we do not have FESEM images of the resulting oxide and thus are left to merely speculate as to what effect this type of anodization would have on the resulting nanopores. Figure 3.12 provides a digital image comparison of the reference sample SV12 with SVDU50a after sputter coating. Although difficult to see the optical characteristics of SVDU50a are somewhat similar to the other thin films except there seems to be an entirely random distribution of purple, greens, yellows and reds occurring in very small individual spots almost as if the iridescence is pixelated across the exposure area.

Once again with out detailed FESEM images of the oxide we can only speculate as to the nature of the oxide resulting from variational down-up anodization. However SVDU50a exhibits a greater initial current value then is typical of samples generated via the variational program, which is significant given that the first half of the two programs are identical. Sample SVDU40, which was produced and sent to CHTM as a sample to evaluated if and when a successfully analysis technique was developed, exhibits a similar

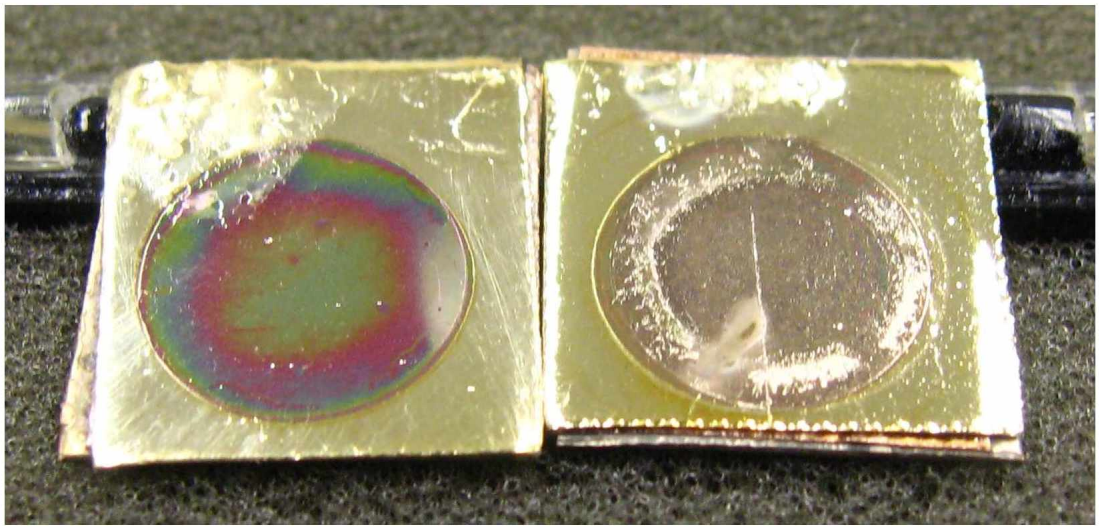

Figure 3.12. Digital image comparing SR12 and Variational Down-Up sample SVDU50a. SR12 (left) and SVDU50a (right) displaying a somewhat pixelated distribution of iridescent colors which are assumed to be related to the underlying thin film characteristics.

current profile but with a much lower initial current value as seen in Figure 3.13.

Interestingly the second half of the current profile for SVDU40 rises well beyond the initial maximum up to about 50 mA. Unfortunately the evaluative samples sent to CHTM had to be raw and thus could not be sputter coated to obtain digital image comparisons. Nevertheless the difference in overall current behavior between SVDU50a and SVDU40, as well as with some of the variational straight samples, remains unexplained at this time.

3.2 Discussion

Figures 3.1 through 3.13 detail the results of variational anodization via sulfuric acid at this time. The moality of the electrolyte was 0.6 M in all cases. The second step anodization length was 12 min in all cases. The electrolyte temperature was seen to vary by less than one degree C in all cases. The applied voltage was a function of time with linear variation according to the previously described programs and served as the experimental control. The current was generally seen to be a function of the applied voltage in most cases with exponential increases and decreases related to barrier layer formation and rates of oxide formation. The system resistance provided by the anodization tank was on the order of 5 kΩ. In the instance of the reference sample an additional system resistance of 1 kΩ was

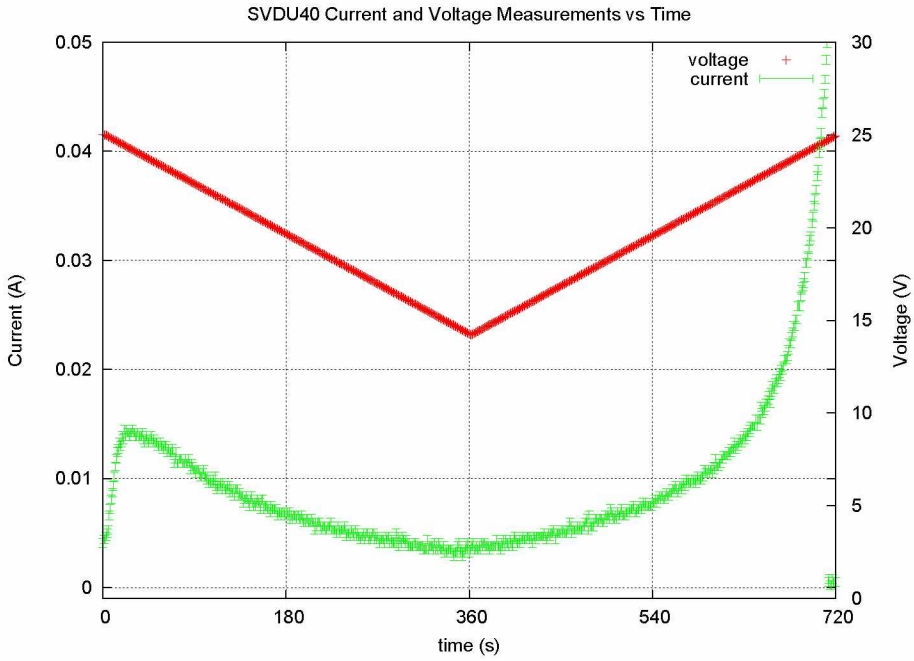

Figure 3.13. Voltage/Current profile of Variational Down-Up sample SVDU40. The initial current was much lower in this trial and its unclear why this is the case. However we can see again the current following the voltage to a minimal value before increasing exponentially as the voltage increases linearly.

incorporated to abate excessive current rise under constant applied voltage translating to a slight reduction in that voltage from 25 V. Additional samples remain with CHTM awaiting successful analysis of the nanopore profile which would lend conclusionary evidence as to the effects, if any, of variational anodization on the subsequent pore geometry.

However we can discuss the recorded data from a different perspective having the real-time records of voltage and current measurements. Using Ohm's Law we can calculate the resistance of the system at each increment and plot this as a function of time. In this case changes in resistance would be directly owing to the extent of oxide produced at a given moment. As alumina is non-conductive, an increasing resistance could be interpreted as an increasing volume of oxide or similarly as a decrease in conductive surface area available for electron transport. Figure 3.14 details the calculated resistance versus time for each of the five samples previously discussed.

The most striking feature here is the instability of the current which is reflected by the

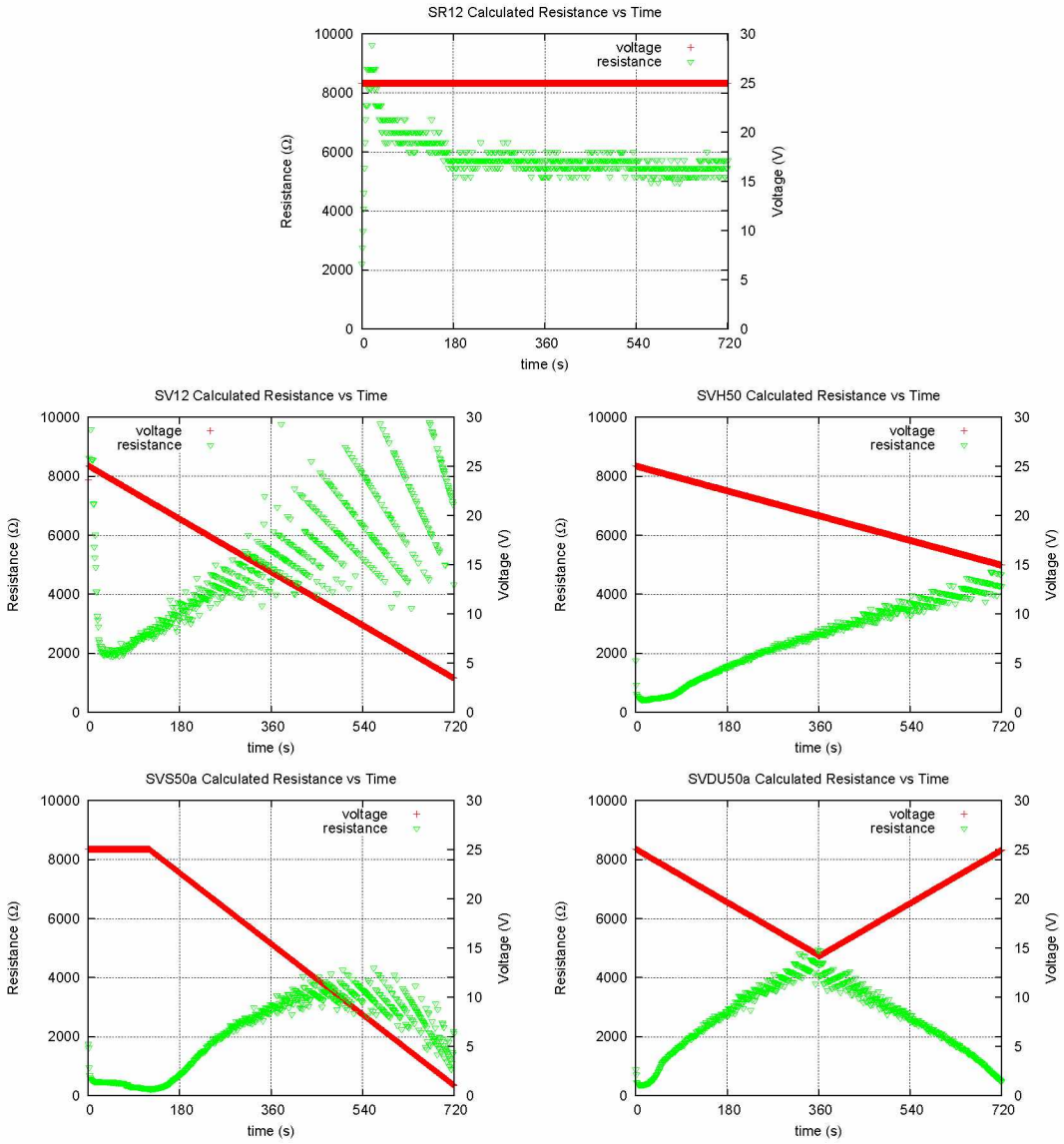

Figure 3.14. Resistance versus time plots. Clockwise from top: reference sample SR12, variational high sample SVH50, variational down-up sample SVDU50a, variational straight sample SVS50a and variational sample SV12.

scattering of the calculated resistances at various points within the experiments. This is a strong indication of a breakdown in the electrochemical reaction, at which point oxide production would be severely hampered if not stopped completely. In such a situation continued exposure to the electrolyte could allow for the unmitigated dissolution of the

existing oxide, which would in turn effectively compromise whatever evidence had been produced as a result of the variational programs.

This seems particularly evident in the case of SV12; as the voltage decreases steadily the current becomes unstable around the two minute mark indicating the possibility of an additional ten minutes during which time oxide production seems reduced and may likely have failed altogether. Even more interesting yet is the voltage level at which point the current becomes unstable. Looking at figure 3.14b-e it is clear that a period of instability exists in each case; and though they occur at different times through out the individual experiments, the instability appears to occur around 20 V in all cases. The optimum voltage for uniform nanofabrication via sulfuric acid was previously stated to be 25 V, and it was also reported that increased deviation from this optimum value resulted in a general loss of uniform distribution of nanopores.[8] The resistance versus time plots would seem to suggest the exploration of a reduction in overall exposure time along with a decrease in the magnitude of variation so as to maintain the overall voltage level equal to or greater than 20 V.

Another point of discussion concerns the optical characteristics of the nanoporous thin film oxide samples and what types of information could be gleaned from interpreting those characteristics. It can be reasonably assumed that the behavior exhibited is resulting principally from two types of interferences: thin film interference and diffractive interference. The optical properties of SV12 is compared to those of SVH40 under florescent white light in Figure 3.15.

The thin film nature of the oxides produced thus far, ranging from 500 nm - 2.5 um and overlaying a highly reflective aluminum substrate, allows for a difference in path length between light reflected off the oxide surface versus light simultaneously penetrating the thin film and reflecting off the underlying substrate. This difference in path length, in combination with the index of refraction and film thickness, will result in constructive interference if it is an integer multiple of the incident wavelength, surmised mathematically via equation 3.1.

$$ndcos(\theta) = m\frac{\lambda}{2} \tag{3.1}$$

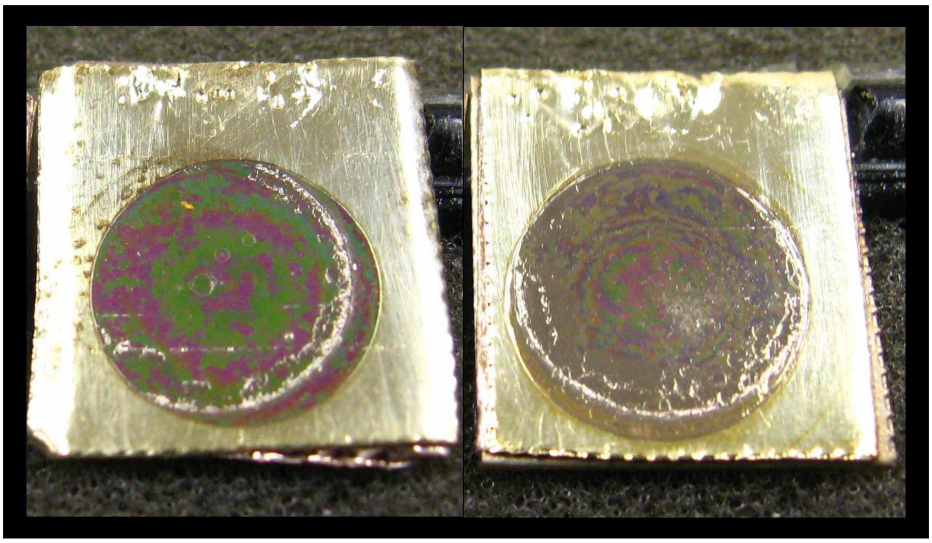

Figure 3.15. Digital image comparing SV12 and SVH40. SV12 (left) and SVH40 (right). Although the difference in optical appearance is clear there may be similar characteristics between the two from a structural point of view.

where n is the index of refraction of aluminum oxide, d is the film thickness, θ is the incident angle, m is the integer order of interference and λ is the wavelength of incident light. In this case we have a good estimate for film thickness given by some of the preliminary images provided by CHTM along with published values for the index of refraction of alumina as a function of incident wavelength such that optical behavior due to thin film interference should be quantifiable to some degree. However this situation is further complicated regarding the digital images provided previously due to the presence of a very thin coating of gold overlaying the thin film oxide. This layer of gold is presumed to have a thickness on the order of tens to hundreds of angstroms and in that case may in fact be entirely opaque with respect to the incident wavelength, however this is not immediately apparent.

Further complification arises from the presence of highly ordered nanopores distributed with a regular spacing which may serve to diffract the light incident on the oxide surface with a given phase change related to the periodicity. In the general case of diffractive interference via a grating or other such optical medium, for example the regular grooving of a common CD, the periodicity of structure or slit spacing is typically on the order of the

incident wavelength, which for visible light will range from 300-700 nm. In such a case the resulting interference pattern will segregate white light into its constituent wavelengths, or colors, as a function of the diffraction angle; given mathematically as

$$dsin(\theta) = m\lambda \tag{3.2}$$

where d is the slit spacing, θ is the diffracted angle, m is the integer order of interference and λ is the wavelength of the diffracted light. However in the case of our samples the slit spacing or periodicity is about 60-70 nm, an order of magnitude less than the range of visible light. Additionally the grating so to speak is two dimensional over the extent of the circular thin film. Under normal conditions, given the incident and diffracted wavelengths, it would be possible to extract the slit spacing or grate spacing of the interfering medium. But in this case it is not immediately apparent in light of the optical characteristics observed, to what degree the interference is owing to thin film interactions versus diffractive interactions; and further more whether or not those interactions could be reasonably separated into majority/minority behaviors. Certainly the inclusion of the gold film does not simplify the problem, however these thin film oxides display similar behaviors even prior to sputter-coating, though it is with a lesser intensity. Further analysis, possibly in the form of optical measurements made mono-chromatically, would be required to quantify the observed effects and could in fact require a theoretical interpretation including dielectric behavior of an imaginary or complex nature.

At this point the principal detractor from conclusionary statements regarding the effects of variational anodization on the nanopore profile is the lack of sufficient images detailing this geometry. However with the few images obtained thus far detailing the oxide porosity from normal incidence, it is possible via secondary image processing to substantiate not only the average pore spacing and diameter but also to visually enhance the hexagonal distribution and compute the subsequent agreement with the 10% porosity rule given by equation 1.4. Figure 3.16 details the oxide resulting from sample SR04 from normal incidence at a magnification of 35 kX.

We can analyze this image with software such as Matlab to extract the relative pore characteristics by interpreting the information contained in the pixels themselves. Spec-

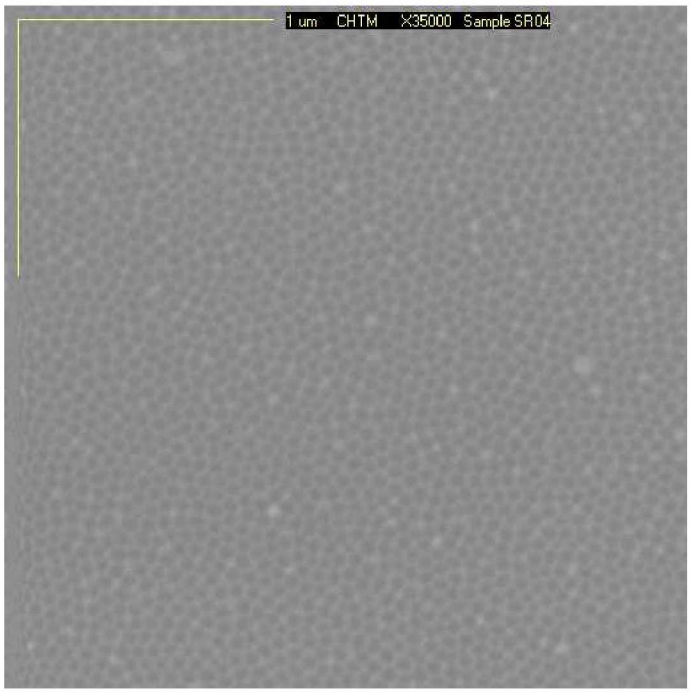

Figure 3.16. Reference sample SR04 at normal incidence. The scale bar is 1 um and the pore spacing appears to be on the order of the pore diameter.

ifying the gray range to a more appropriate level enhances the visual appearance while providing sharper pore boundaries to be used in further analysis as seen in figure 3.17. Cropping a more representative section of this image excluding the scale bar and the aberration along the left side provides a good image for further analysis.

We begin by looking at a gray value plot of a horizontal slice across the image. When plotting the image data in this way the y-axis is interpreted as the gray intensity or gray value with darker shades registering higher values versus lighter shades. The x-axis is just that, the x position of each pixel from the left side of the image to the right. Plotting various horizontal slices of the cropped image in figure 3.17 we find a similar signature represented by one such plot in figure 3.18 where each peak is approximating the location of a dark pore. We can see that there are about three to four peaks per 50 pixels. Extracting the length of the scale bar from the original image in terms of pixels allows us to relate pixel count to a length in nanometers. In this case the 1 um scale bar occupied 189 pixels such that each pixel represents about 5.3 nm. This lends and average pore separation between

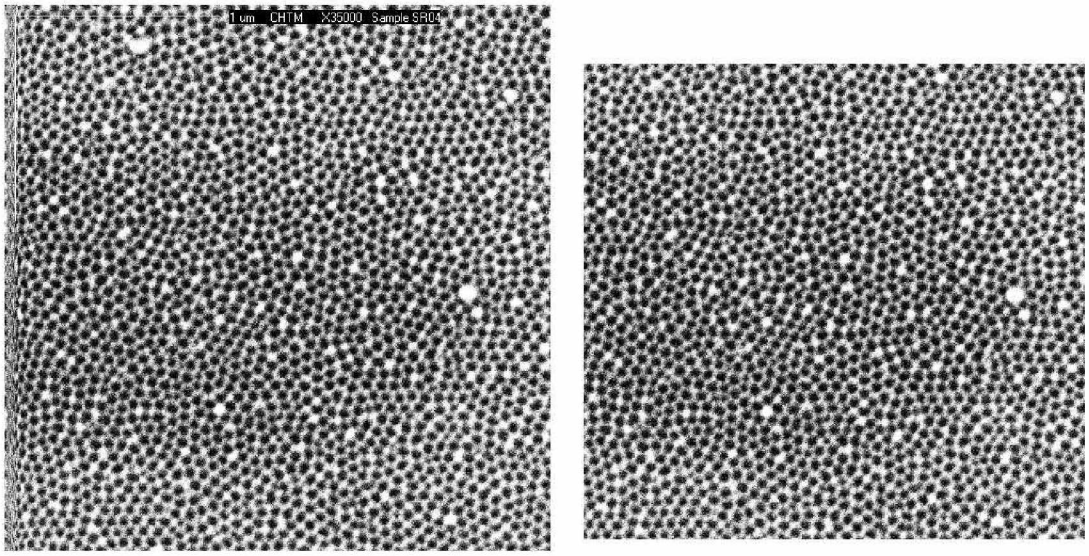

Figure 3.17. Contrasting and cropping of the image presented in figure 3.16. (Left) Gray scale enhancement of the image results in pore boundaries which are sharper allowing for further image processing. (Right) Cropping a more representative section excluding the scale bar and artifacts of the original image.

60-70 nm. This value is D_int seen in equation 1.4 and if combined with the pore radius would yield the percentage of porosity which could then be compared to the 10% rule for a hexagonal distribution.

To obtain an average value for the pore radius we can zoom in on a region of the cropped image above and measure the number of light pixels representing the intervening oxide between pores. Averaging a number of these measurements yields a value for the distance between pore edges. Subtracting this number from the inter-pore distance found previously yields an average value for the pore diameter and subsequently the pore radius. Figure 3.19 details such a zoomed image. It is clear to see that indeed the pores seem to align themselves along the diagonal, a property indicative of hexagonal ordering. The red and green marks denote pixel measurements along the horizontal and diagonal directions respectively. Averaging a number of these measurements yields an intervening oxide length of about 4.5 pixels. Using the aforementioned conversion of 5.3 $\frac{nm}{px}$ this is equivalent to a length of about 24 nm. Subtracting this from our average inter-pore distance of 65 nm

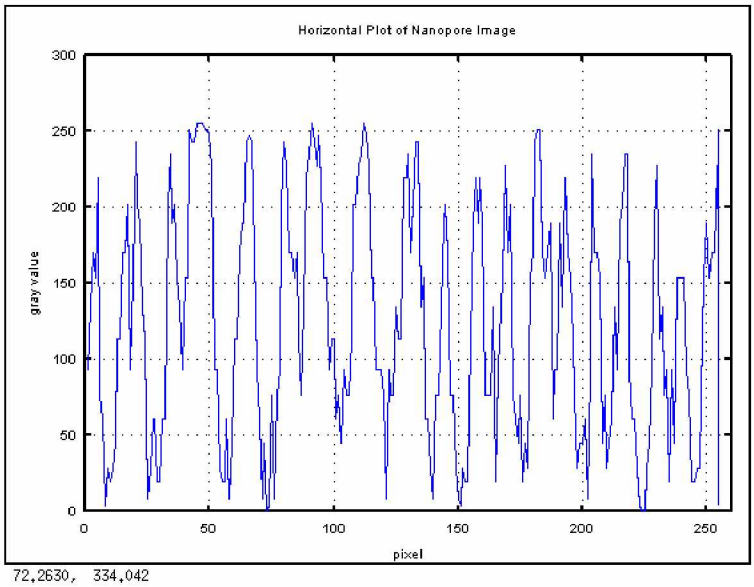

Figure 3.18. Typical plot of a horizontal slice through the cropped image. The peaks are corresponding to pore locations and display a fairly regular interval.

yields a pore diameter of 41 nm and thus an average pore radius of about 20.5 nm. The 10% porosity rule states that the squared ratio of the pore radius to the inter-pore spacing will equal about 10% for hexagonal distributions of ordered nanopores. Using our values this ratio is found to equal 0.0994 or otherwise 10% thus satisfying the 10% porosity rule and verifying that indeed the nanopores are uniformly ordered with a hexagonal distribution.

With out detailed cross sectional images of the nanopore profile we can only draw a limited number of conclusions at this time based on the evidence at hand. Firstly, via the preliminary images courtesy of CHTM detailed in Figures 3.3 and 3.5, we can state that both our two-step anodization method, and the modification of that method incorporating variational anodization have resulted in the fabrication of nanoporous aluminum oxide. With respect to the reference program we can state that the square of the ratio of the pore radius to the inter-pore diameter is 10% there by satisfying the 10% porosity rule for hexagonally ordered distributions of nanopores.

Additionally we can state that between the reference sample SR12 and the variational sample SV12, there is a difference in the oxide thickness of approximately 1.5 um with film thicknesses appearing to be on the order of 2 um and 0.5 um respectively. This difference is

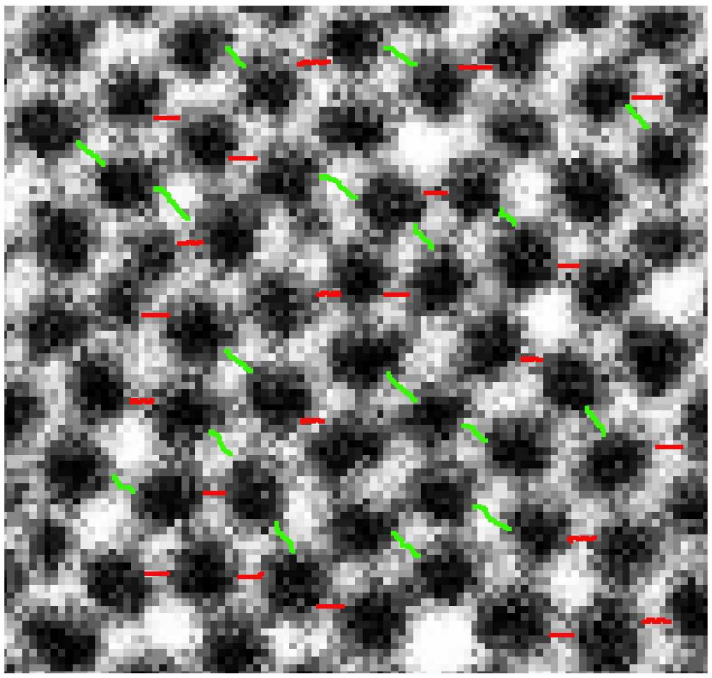

Figure 3.19. Zoomed version of the cropped image. The diagonal alignment of the nanopores further suggests a hexagonal distribution, however we can average a number of measurements of the intervening oxide along the horizontal and diagonal directions, marked by the red and green lines respectively, to figure the average length of the intervening oxide.

further evidenced by the distinction in optical properties given by figure 3.5d in which the two samples, having been sputter coated with gold simultaneously, where then imaged simultaneously with a digital camera under identical conditions. Although further analysis would be required to state whether these differences were owning to thin film versus diffractive interference, or a combination of both, we can nevertheless acknowledge the difference and know that it speaks to a range of thin film oxide characteristics effected by the various anodization programs devised in this work.

Finally we can see from figure 3.14 that the current tends to consistently destabilize at or slightly below 20 V. This suggests that a portion of the variational programs may in fact not be producing additional oxide beyond this point and what already exists could be

dissolved away under continued exposure to the electrolyte. Future experiments should take note of this fact and adjust the linear variation in potential difference accordingly. Although a finer time step is desirable to emulate a linear change, this factor is predetermined by the programmable power-supply employed and in our case would necessitate a similar level of variation but with an experiment length more on the order of five minutes or less.

Chapter 4
Conclusions

The goal of this work was to investigate the effects of a time varied potential difference on the two-step anodization method, termed variational anodization, with the express purpose of developing a technique by which the nanopore geometry could be tailored in process and conically profiled nanopores uniformly assembled in thin film aluminum oxide templates. Nanofabrication via anodization has been explored and refined with the two-step method originally developed in the mid 1990s having been extended to multi-step anodization, in addition to various post-processing techniques, in recent years.[3] The latest works have shown that the tailoring of pore profiles can be realized via current modulation in a technique termed cyclic anodization.[23] This technique along with many others encompasses a burgeoning field in applied physics and materials science, generally referred to as nanosculpture or nanosculpting, which continues to grow and expand in a direction towards fabrication of increasingly complex and refined nanostructures. This work was intended to make a small contribution towards this evolution via a technique termed variational anodization.

In the end however it must be admitted that we fell short of this goal. Worse yet is the fact that although variational anodization did produce uniformly ordered nanoporous thin films, its effect on the nanopore profile is inconclusive at this time. We can not unequivocally state that variational anodization did or did not result in a change of pore geometry from the standard cylindrical shape to a conically shaped profile or otherwise. With out the detailed analysis provided by high quality FESEM images of the alumina cross-section exposing the nanopore profiles, our results are qualitative at best. CHTM continues working on our behalf to obtain such conclusionary evidence. But for the time being it must remain that the effects of variational anodization on nanopore geometry remain unknown despite our efforts.

4.1 Summary of Results

Figures 3.1 through 3.19 detail the results of this work at the present time. Unfortunately none of the evidence put forth can adequately describe the effects, if any, of variational anodization on the subsequent nanopore geometry. Nevertheless, figures 3.3 and 3.5 detail

the presence of nanoporous thin film oxide resulting from the standard two-step anodization method as well as the variational method described previously. Nanopores resulting from the reference program display a close-packed hexagonal ordering with a porosity in agreement with the 10% rule.

The observations made in this investigation take the form of voltage and current profiles recorded in real time and exported to secondary plotting programs. The linearly time dependent applied voltage was taken as the experimental control with the subsequent current taken as the dependent variable. Current measurements included a systematic uncertainty of 0.4 mA owing to the limit of probe sensitivity. In general the current profiles exhibited a familiar trend with initial exponential increases during barrier layer formation followed by non-linear decreases dependent on the variably applied voltage. However figure 3.14 reveals a consistent instablility in the current slightly below 20 V indicating a breakdown of the electrochemical reaction at voltages below this value. This could be remedied with a shorter experiment length on the order of five minutes and varying the applied voltage with in the stable range.

4.2 Future Applications

Although this work as relates to the effects of variational anodization on the resulting nanopore profile remains inconclusive at this time, we continue working with CHTM in the hopes that they can successfully image the thin film cross section and provide us with the definitive evidence needed to at some point in the future, either refute or support variational anodization. If and when this analysis is completed, and if it turns out that variational anodization does in effect modulate the nanopore profile, additional samples would be provided including variational anodization in oxalic acid to further verify this conclusion. On the other hand, if variational anodization turns out to have no measurable effect on pore geometry then that result would be stated explicitly such that future research could be informed of this conclusion.

In the mean time however we have presented the qualitative results of this investigation and though not entirely satisfied with the outcome, we remain supportive of the idea and the level of effort put forth in its execution. A great deal was learned during this project, techniques where developed, skills acquired and collaborations formed. If varia-

tional anodization ultimately proves to be a fruitless methodology within the greater body of knowledge it will not be for the lack of trying. And I would remain grateful for the experience of concluding as much.

Bibliography

[1] R. Feynman. There's Plenty of Room at the Bottom. Online, 1960.

[2] K. Wolter. Institute of Semiconductor Electronics: Photovoltaics. Online.

[3] R. Krishnan. *Templated Self-Assembly of Nanoporous Alumina*. PhD thesis, Department of Materials Science and Engineering, MIT, 2005.

[4] S. Sen and N. A. Kouklin. *Nanofabrication: Fundamentals and Applications*, chapter 5. World Scientific, 2006.

[5] A. Pereira, D. Grojo, and M. Chaker. *Small*, 4(5), 2008. online.

[6] M. Va'zqueza, K. R. Pirotaa, and D. Navasa. *Magnetism and Magnetic Materials*, 320, 2008. Alnstituto de Ciencia de Materiales. CSIC, Madrid, Spain.

[7] H. Masuda and K. Fukuda. *Science*, Vol 268(5216), 1995.

[8] O. Jessensky, F. Muller, and U. Gosele. *App. Phys. Lett.*, 72(10), 9 Mar. 1998.

[9] J. O'Sullivan and G. Wood. *Proceedings of the Rolyal Society A*, (317):511, 1970.

[10] S. Shingubara. *Nanoparticle Research*, Vol 5, 2003. Netherlands.

[11] K. Nielsch, J. Choi, and K. Schwim. *Nano Letters*, 2(7), 2002.

[12] W. Lee, K. Schwirn, and M. Steinhart. *Nature Nanotechnology*, 3, 2008.

[13] T. Gao, J.C. Fan, and G.W. Meng. *Thin Solid Films*, Vol 401, 2001. Institute of Solid State Physics. Chinese Academy of Sciences, Hefei PR China.

[14] G. K. Singh, A. A. Golovin, and I. S. Aranson. *Physical Review B*, Vol 73, 2006.

[15] Son H. Le. *Online*, (Delft University of Technology), 2008.

[16] S. Z. Chu, K. Wada, and S. Inoue. *Advanced Materials*, 2005.

[17] T. Nagaura. *Electrochemistry Communications*, 10:681–685, 2008.

[18] T. Nagaura. *Electrochimica Acta*, 53:2109–2114, 2008.

[19] Y. Yamauchi, T. Nagaura, and K. Takai. *Journal of Physical Chemistry C*, (113):9632–9637, 2009.

[20] Y. Yamauchi. *American Chemical Society*, (130):10165–10170, 2008.

[21] W. Lee and K. Nielsch. *online*, 2007. Max-Planck-Institute.

[22] D. Regonini, C.R. Bowen, and D. Allsopp. *online*. Materials Research Centre, Department of Mechanical Engineering, University of Bath. UK. Multi-material Micro Manufacture.

[23] D. Losic, M. Lillo, and D. Losic Jr. *Wiley InterScience- Small*, 2009.

[24] R. Newman. A Practical Guide to Anodizing Aluminum at Home. Self, Feb. 2009.

[25] A. Rauf, M. Mehmood, M. A. Rasheed, and M. Aslam. *Solid State Electrochemistry*, 2008.